repiSalud
Repositorio Institucional en Salud

This is the pre-print version of the following article:

González-Cofrade, Laura; Green, Jack P; Cuadrado, Irene; Amesty, Ángel; Oramas-Royo, Sandra; Brough, David; Estévez-Braun, Ana; Hortelano, Sonsoles; Las Heras, Beatriz de. **Phenolic and quinone methide nor-triterpenes as selective NLRP3 inflammasome inhibitors.** Bioorg Chem. 2023 Mar:132:106362.
which has been published in final form at

https://doi.org/10.1016/j.bioorg.2023.106362

Phenolic and quinone methide *nor*-triterpenes as selective NLRP3 inflammasome inhibitors.

Laura González-Cofrade[a], Jack P. Green[b,c], Irene Cuadrado[a], Ángel Amesty[d], Sandra Oramas-Royo[d], David Brough[b,c], Ana Estévez-Braun[*,d], Sonsoles Hortelano[*,e], Beatriz de las Heras[*,a]

[a] Departamento de Farmacología, Farmacognosia y Botánica, Facultad de Farmacia, Universidad Complutense de Madrid (UCM), Plaza Ramón y Cajal s/n, 28040 Madrid, Spain.

[b]Division of Neuroscience, School of Biological Sciences, Faculty of Biology, Medicine and Health, Manchester Academic Health Science Centre, University of Manchester, Manchester, United Kingdom.

[c]Lydia Becker Institute of Immunology and Inflammation, University of Manchester, Manchester, United Kingdom.

[d]Departamento de Química Orgánica, Instituto Universitario de Bio-Orgánica Antonio González, Universidad de La Laguna, Avda. Astrofísico Francisco Sánchez 2, 38206 La Laguna, Tenerife, Spain.

[e]Unidad de Terapias Farmacológicas, Área de Genética Humana, Instituto de Investigación de Enfermedades Raras (IIER), Instituto de Salud Carlos III, Carretera de Majadahonda-Pozuelo Km 2, 28220 Madrid, Spain.

***Corresponding Authors**
*E-mail (B. de las Heras): lasheras@ucm.es Tel: +34 913941608
*E-mail (S. Hortelano): shortelano@isciii.es Tel: +34918223291
*E-mail (A. Estévez-Braun): aestebra@ull.edu.es Tel: +34 922318576

Abstract

Dysregulated inflammasome activity, particularly of the NLRP3 inflammasome, is associated with the development of several inflammatory diseases. The study of molecules directly targeting NLRP3 is an emerging field in the discovery of new therapeutic compounds for the treatment of inflammatory disorders. Friedelane triterpenes are biologically active phytochemicals having a wide range of activities including anti-inflammatory effects. In this work, we evaluated the potential anti-inflammatory activity of phenolic and quinonemethide *nor*-triterpenes (**1-11**) isolated from *Maytenus retusa* and some semisynthetic derivatives (**12-16**) through inhibition of the NLRP3 inflammasome in macrophages. Among them, we found that triterpenes **6** and **14** were the most potent, showing markedly reduced caspase-1 activity, IL-1β secretion (IC_{50} = 1.15 μM and 0.19 μM, respectively), and pyroptosis (IC_{50} = 2.21 μM and 0.13 μM, respectively). Further characterization confirmed their selective inhibition of NLRP3 inflammasome in both canonical and non-canonical activation pathways with no effects on AIM2 or NLRC4 inflammasome activation.

Key words. *Nor*-friedelane triterpenes, *Maytenus retusa*, NLRP3 inflammasome, ASC, pyroptosis, IL-1β, macrophages

***Abbreviations*:** AIM2, absent in melanoma 2; ASC, apoptosis-associated speck-like protein containing a caspase recruitment domain (CARD); ATP, adenosine triphosphate; BMDMs, bone-marrow derived macrophages; DSS, disuccinimidyl suberate; DMEM, Dulbecco's modified Eagle medium; GSDMD, gasdermin D; IL, interleukin; IMQ, imiquimod; LDH, lactate dehydrogenase; LPS, lipopolysaccharide; MTT, 3-(4,5-dimethylthiazol-2-yl)-2,5-diphenyltetrazolium bromide; Nig, nigericin; NLRC4, NOD-like receptor family CARD domain containing 4; NLRP3, NOD-like receptor family pyrin domain containing 3; TCA, trichloroacetic acid.

1. Introduction

Inflammation is an immune response that protects the host from infection or tissue injury. It is initiated by innate immune cells such as macrophages upon detection of pathogen-associated molecular patterns (PAMPs) or damage-associated molecular patterns (DAMPs) by pattern recognition receptors (PRRs). In this context, inflammasomes are PRR dependent multiprotein complexes that have emerged as pivotal regulators of inflammatory responses [1]. Inflammasomes are assembled in the cytosol by PRRs including NOD-like receptor (NLR) family members such as NLR family pyrin domain containing 1 (NLRP1), NLRP3 and NLR family CARD domain containing 4 (NLRC4), as well as other non-NLR receptors, such as the double-stranded DNA (dsDNA) sensor absent in melanoma 2 (AIM2), and pyrin [2, 3].

NLRP3 forms the best characterized inflammasome and is formed by the sensor NLRP3, the adaptor protein ASC (apoptosis-associated speck-like protein containing a caspase recruitment domain) and the effector enzyme caspase-1 [4]. Once stimulated, NLRP3 recruits ASC causing its oligomerization to form a large complex termed an 'ASC speck' [5]. This complex acts as a platform for autocatalytic activation of caspase-1, which cleaves pro-interleukin (IL)-1β and pro-IL-18 to mature secreted forms (IL-1β and IL-18). Caspase-1 activation also results in the cleavage of gasdermin D (GSDMD) to produce GSDMD-N terminal fragments that form pores in the plasma membrane, leading to a rapid lytic cell death named pyroptosis [6-8]. IL-1β and IL-18 together with pyroptosis induce robust inflammatory responses to confer host protection [9].

Several pathways of NLRP3 inflammasome activation are described including canonical, non-canonical, and alternative pathways [10]. Canonical NLRP3 inflammasome activation is the most studied pathway and is regulated through a two-step process. An initial priming signal mediated by NF-κB activation leads to pro-IL-1β and NLRP3 expression, and a subsequent second signal is responsible for inflammasome assembly and activation [11]. The second signal can be triggered by many different stimuli, including K^+ ionophores such as nigericin, extracellular danger signals such as ATP and particulate matter such as silica or asbestos, among others [12]. Several downstream molecular events have been proposed for NLRP3 activation and inflammasome formation, including potassium (K^+) efflux-dependent and efflux-independent mechanisms involved in organelle disfunction [13-15].

Notably, emerging studies have shown that uncontrolled NLRP3 inflammasome activation is involved in the pathogenesis of various inflammatory diseases, such as autoimmune and autoinflammatory disorders, cardiovascular, metabolic and neurodegenerative diseases, and cancer [16-19]. The NLRP3 inflammasome also plays a critical role in the inappropriate hyperinflammatory response observed in severe COVID-19 cases [20]. Thus, the NLRP3 inflammasome constitutes a potential target for the treatment of these pathologies. Nevertheless,

although some small molecule inhibitors are described showing promising therapeutic activity, there is still a clinical need to develop further NLRP3 inhibitors [21, 22].

In the search for new therapeutic agents, natural products and their derivatives have been traditionally explored as a successful source [23]. Among them, terpenes are a structurally diverse group of compounds with remarkable broad pharmacological potential including anti-inflammatory, antibacterial, anticancer and antioxidant activities [24-32].

Triterpenes are plant secondary metabolites containing 30 carbon atoms. They have been isolated as active constituents of various plants and are classified into two main groups: tetracyclic and pentacyclic triterpenes [33]. Interestingly, pentacyclic triterpenes have gained attention as multi-target compounds able to modulate different molecular and cellular pathways, with great therapeutic potential in inflammatory diseases [34-38].

Friedelane-type triterpenes, the most abundant pentacyclic triterpenes isolated from *Maytenus* species (Celastraceae), have known anti-inflammatory properties [35]. Particularly, celastrol, a quinone methide *nor*-triterpene, exhibits anti-inflammatory activities via inhibition of NLRP3 inflammasome activation suggesting that these compounds might be useful for the treatment of NLRP3-associated diseases [39-45].

Previously, several new nor-triterpenes isolated from the root bark of *Maytenus retusa* have been reported to exhibit cytotoxicity against human tumor cell lines [46], however, their anti-inflammatory effects remained unexplored. Thereby, this study aimed to find potent and selective NLRP3 inflammasome inhibitors from this type of compounds and some derivatives. To this end, a set of phenolic *nor*-triterpenes [zeylasteral (**1**), macrocarpin a (**2**), 6-oxotingenol (**3**), 3-methoxy-6-oxotingenol-23-oic acid (**4**), 23-*nor*-blepharodol (**5**), 3-*O*-methyl-22-β-hydroxy-6-oxotingenol (**6**)], the quinone-methide triterpenes pristimerin (**7**), tingenone (**8**), 20β-hydroxy-tingenone (**9**), 22β-hydroxytingenone (**10**), the triterpene cangoronin (**11**), and five semisynthetic nor-triterpenequinone derivatives [19-α-bromo-22β-hydroxytingenone (**12**), 18,19-dehydrotingenone (**13**), 11-β-bromo-tingenone (**14**), tingenone-oxime (**15**) and 22β-hydroxy-tingenone-oxime (**16**)] were evaluated as inflammasome inhibitors.

Our findings indicated that triterpenes **6** and **14** inhibited NLRP3 inflammasome activation, and lacked any inhibitory effect on AIM2 and NLRC4 inflammasomes.

2. Material and methods

2.1. Chemistry

Triterpenes **1**-**11** were isolated from the root bark of *Maytenus retusa* as previously described [46] and their structures ratified by NMR spectroscopy, MS spectrometry, and by comparison with the published data.

2.1.1. Preparation of 19α-bromo-22β-hydroxy-tingenone (12) and 18,19-dehydrotingenone (13).

A solution of 342 mg (0.78 mmol) of 22β-hydroxy-tingenone **(10)** dissolved in 50 mL of dry CH_2Cl_2 under N_2 atmosphere, was treated with 1.17 mL (1.5 equiv) of 1M BBr_3 solution in CH_2Cl_2. The reaction mixture was stirred at 0 ºC until disappearance of the starting triterpene (30 min). Then, 50 mL of cold water was added, and the mixture was stirred for additional 30 min. The organic layer was separated, and the aqueous layer was extracted several times with CH_2Cl_2. The combined organic extracts were dried over anhydrous $MgSO_4$. The solvent was evaporated under vacuum and the residue was purified by Sephadex LH-20 chromatography (hexane/$CHCl_3$/MeOH; (2:1:1)) followed by flash chromatography using hexane/EtOAc (7:3) to yield 111 mg (27%) of compound **12** and 130 mg (40%) of compound **13**.

19α-bromo-22β-hydroxy-tingenone (**12**). Amorphous orange solid; $[\alpha]_D^{20}$ -11.95 (*c* 0.8, $CHCl_3$); ^{1}H NMR ($CDCl_3$) δ: 0.50 (3H, s, Me-27); 1.16 (3H, d, *J*= 5.9 Hz, Me-30); 1.29 (3H, s, Me-26); 1.36 (3H, s, Me-28); 1.44 (3H, s, Me-25); 2.20 (3H, s, Me-23); 2.61 (1H, m, H-20); 3.70 (1H, d, *J*= 2.9 Hz, H-22); 4.03 (1H, dd, J_1= 2.6, J_2= 10.2 Hz, H-19); 6.32 (1H, d, *J*= 7.2 Hz, H-7); 6.50 (1H, d, *J*= 1.3 Hz, H-1); 7.00 (1H, dd, J_1= 1.3, J_2= 7.1 Hz, H-6); ^{13}C NMR ($CDCl_3$) δ: 10.2 (CH_3, C-23); 20.3 (CH_3, C-27); 20.9 (CH_3, C-30); 21.7 (CH_3, C-26); 27.9 (CH_2, C-16); 28.0 (CH_2, C-15); 28.9 (CH_2, C-12); 30.9 (CH_3, C-28); 33.4 (CH_2, C-11); 37.9 (CH_3, C-25); 40.0 (CH, C-20); 40.4 (C, C-14); 42.7 (C, C-9); 44.4 (C, C-13); 45.5 (C, C-17); 48.7 (CH, C-18); 76.6 (CH, C-19); 77.2 (CH, C-22); 118.6 (CH, C-7); 119.6 (CH, C-1); 127.7 (C, C-5); 133.7 (CH, C-6); 146.1 (C, C-4); 149.5 (C, C-3); 164.1 (C, C-10); 167.9 (C, C-8); 178.4 (C, C-2); 216.5 (C, C-21). EIMS m/z 436 (M^+-Br) (80), 422 (51), 253 (60), 239 (58), 227 (55), 202 (100), 187 (30), 95 (11), 55 (9); HREIMS calcd for $C_{28}H_{36}O_4$ 436.2614, found 436.2695; IR (film) ν_{max} 3568, 3354, 2927, 2872, 2360, 1734, 1699, 1638, 1595, 1551, 1515, 1440, 1379, 1288, 1222, 1192, 1084, 999, 869, 803, 754, 665 cm^{-1}.

18,19-dehydrotingenone (**13**). Brown amorphous solid; $[\alpha]_D^{20}$ -221.7 (*c* 1.5, $CHCl_3$); ^{1}H NMR ($CDCl_3$) δ: 0.65 (3H, s, Me-28); 1.09 (3H, s, Me-27); 1.39 (3H, s, Me-26); 1.50 (3H, s, Me-25); 1.83 (3H, s, Me-30); 2.20 (3H, s, Me-23); 2.34 (1H, d, *J*= 5.3 Hz, H-18); 6.34 (1H, d, *J*= 7.2 Hz, H-7); 6.51 (1H, bs, H-1); 6.67 (1H, d, *J*= 5.6 Hz, H-19); 7.01 (1H, d, *J*= 6.9 Hz, H-6); ^{13}C NMR ($CDCl_3$) δ: 10.0 (CH_3, C-23); 15.8 (CH_3, C-30); 17.1 (CH_3, C-28); 20.9 (CH_3, C-26); 28.2 (CH_2, C-15); 29.4 (CH_2, C-16); 32.7 (CH_3, C-27); 33.2 (C, C-17); 33.4 (CH_2, C-11); 34.1 (CH_2, C-12); 38.6 (CH_3, C-25); 41.5 (C, C-13); 42.6 (C, C-14); 43.1 (C, C-9); 47.9 (CH, C-18); 48.5 (CH_2, C-22); 116.9 (C, C-4); 117.8 (CH, C-7); 119.6 (CH, C-1); 127.5 (C, C-5); 133.4 (CH, C-6); 135.9

(C, C-20); 144.7 (CH, C-19); 145.8 (C, C-3); 164.2 (C, C-10); 167.2 (C, C-8); 178.2 (C, C-2); 199.5 (C, C-21). EIMS *m/z* 418 (M^+) (97), 404 (31), 281 (15), 268 (36), 253 (29), 241 (83), 227 (39), 215 (12), 201 (100), 187 (18), 135 (19), 123 (23), 95 (11), 55(8); HREIMS calcd for $C_{28}H_{34}O_3$ 418.2508, found 418.2508; IR (film) ν_{max} 3311, 2951, 2873, 1707, 1665, 1594, 1550, 1516, 1438, 1377, 1287, 1218, 1187, 1086, 1038, 869, 803, 754, 665 cm^{-1}.

2.1.2. Preparation of 11-β-bromo tingenone (14)

A solution of 70 mg (0.17 mmol) of tingenone **(8)** in 10 mL of CH_2Cl_2 was treated with 60 mg (2 equiv) of NBS at rt. The reaction mixture was stirred for 2 h, until disappearance of starting triterpene. Then the solvent was removed under vacuum, and the residue was purified by preparative-TLC using CH_2Cl_2/EtOAc (3:2) 18 mg (21%) of compound **(14)** were obtained as an amorphous orange solid; $[\alpha]_D^{20}$ +14.4 (*c* 0.5, $CHCl_3$); ^{1}H NMR ($CDCl_3$) δ: 0.99 (3H, s, Me-28); 1.00 (3H, d, *J*= 5.2 Hz, Me-30); 1.01 (3H, s, Me-27); 1.38 (3H, s, Me-26); 1.76 (3H, s, Me-25); 2.20 (3H, s, Me-23); 4.81 (1H, dd, J_1= 6.7 Hz, J_2= 12.0 Hz, H-11); 6.28 (1H, d, *J*= 7.0 Hz, H-7); 6.89 (1H, d, *J*= 7.0 Hz, H-6); 7.35 (1H, s, H-1); ^{13}C NMR ($CDCl_3$) δ: 10.2 (CH_3, C-23); 14.9 (CH_3, C-30); 19.5 (CH_3, C-27); 21.2 (CH_3, C-26); 28.3 (CH_2, C-15); 31.7 (CH_2, C-16); 32.0 (CH_3, C-28); 35.0 (CH_2, C-19); 37.6 (CH_3, C-25); 38.1 (s, C-13); 41.6 (CH, C-18); 42.4 (C, C-14); 42.8 (CH, C-20); 44.3 (C, C-17); 44.9 (CH_2, C-12); 46.8 (s, C-9); 51.6 (CH_2, C-22); 58.3 (CH, C-11); 117.9 (C, C-4); 118.4 (CH, C-7); 121.1 (CH, C-1); 129.6 (C, C-5); 131.4 (CH, C-6); 152.9 (C, C-3); 162.7 (C, C-10); 165.4 (C, C-8); 178.3 (C, C-2); 212.8 (C, C-21); EIMS *m/z* 498 (M^+) (1), 418 (39), 404 (100), 389 (16), 317 (10), 279 (15), 265 (35), 251 (95), 239 (18), 227 (19), 201 (23), 165 (6), 123 (5), 107 (5), 95 (8), 55 (9); HREIMS 498.1801 (calcd for $C_{28}H_{35}{}^{79}BrO_3$ 498.1770), 500.1778 (calcd for $C_{28}H_{35}{}^{81}BrO_3$ 500.1749); IR (film) ν_{max} 3322, 2955, 2855, 1711, 1602, 1519, 1435, 1377, 1286, 1173, 1093, 840, 708 cm^{-1}.

2.1.3. Preparation of tingenone oxime (15).

A solution of 157 mg (0.37 mmoles) of tingenone (**8**) in 15 mL of EtOH was treated with 77.9 mg (3 equiv) of hydroxylamine hydrochloride and 61.3 mg (2 equiv) of sodium acetate dissolved in 2 mL of water. The reaction mixture was heated under reflux for 24 h. Filtration of the solid formed yielded 155 mg (96%) of (**15**) as an amorphous orange solid. $[\alpha]_D^{20}$ -49.1 (*c* 3.5, $CHCl_3$); ^{1}H NMR ($CDCl_3$) δ: 7.05 (1H, d, *J*= 7.0 Hz, H-6); 6.53 (1H, bs, H-1); 6.37 (1H, d, *J*= 7.2 Hz, H-7); 2.45 (1H, m, H-20); 2.22 (3H, s, Me-23); 1.47 (3H, s, Me-25); 1.31 (3H, s, Me-26); 1.06 (3H, d, *J*= 6.2 Hz, Me-30); 1.02 (3H, s, Me-28); 0.86 (3H, s, Me-27); ^{13}C NMR ($CDCl_3$) δ: 10.0 (CH_3, C-23); 16.7 (CH_3, C-30); 20.0 (CH_3, C-27); 21.3 (CH_3, C-26); 28.4 (CH_2, C-15); 29.5 (CH_3, C-17); 29.6 (CH_2, C-12); 31.9 (CH_3, C-28); 32.0 (CH_2, C-19); 33.4 (CH, C-20); 33.5 (CH_2, C-11); 34.8 (CH_2, C-16); 35.0 (CH_2, C-22); 35.1 (C, C-13); 38.7 (CH_3, C-25); 42.6 (C, C-9); 43.4 (CH, C-18); 44.5 (C, C-14); 117.1 (C, C-4); 117.9 (CH, C-7); 119.5 (CH, C-1); 127.4 (C, C-5); 133.7 (CH, C-6); 145.8 (C, C-3); 162.3 (C, C-21); 164.6 (C, C-10); 169.2 (C, C-8); 178.2 (C, C-2).

EIMS *m/z* 435 (M^+) (45), 421 (35), 405 (16), 390 (11), 253 (25), 241 (45), 227 (51), 202 (100), 187 (17), 175 (14), 134 (10), 122 (11), 107 (13), 95 (15), 55 (11); HREIMS calcd for $C_{28}H_{37}NO_3$ 435.2773, found 435.2788; IR (film) ν_{max} 3345, 2929, 1710, 1649, 1588, 1445, 1378, 1217, 1083, 940, 756, 665 cm^{-1}.

2.1.4. Preparation of 22*β*-hydroxytingenone oxime (16).

A solution of 203 mg (0.46 mmol) of 22*β*-hydroxytingenone **(10)** in 20 mL of ethanol was treated with 97 mg (3 equiv) of hydroxylamine hydrochloride and 76 mg (2 equiv) of sodium acetate NaOAc dissolved in 4 mL of water. The reaction mixture was stirred for 24h at rt, the white precipitate formed was filtered and purified by flash chromatography using a mixture of hexane/EtOAc of increasing polarity (from 20% to 40%) to yield 136 mg (66%) of compound **16** as an amorphous orange solid. $[\alpha]_D^{20}$ -240.6 (*c* 0.3, $CHCl_3$); ^{1}H NMR ($CDCl_3$) δ: 7.06 (1H, dd, J_1= 0.8, J_2= 7.0 Hz, H-6); 6.53 (1H, d, *J*= 0.8 Hz, H-1); 6.37 (1H, d, *J*= 7.0 Hz, H-7); 4.78 (1H, bs, H-22); 2.22 (3H, s, Me-23); 1.48 (3H, s, Me-25); 1.33 (3H, s, Me-26); 1.15 (3H, s, Me-27); 1.02 (3H, d, *J*= 6.2 Hz, Me-30); 0.81 (3H, s, Me-28); ^{13}C NMR ($CDCl_3$) δ: 10.13 (CH_3, C-23); 17.1 (CH_3, C-30); 20.4 (CH_3, C-26); 21.5 (CH_3, C-27); 25.8 (CH_3, Me-28); 26.9 (CH_2, C-15); 28.4 (CH_2, C-12); 29.8 (CH_2, C-16); 33.3 (CH_2, C-19); 34.0 (CH_2, C-11); 36.0 (CH, C-20); 39.0 (c, C-25); 40.38 (C, C-13); 42.7 (C, C-9); 43.4 (C, C-17); 44.3 (C, C-14); 45.4 (CH, C-18); 77.9 (CH, C-22); 117.7 (C, C-4); 118.1 (CH, C-7); 119.7 (CH, C-1); 127.6 (C, C-5); 134.2 (CH, C-6); 146.1 (C, C-3); 162.1 (C, CNOH); 164.9 (C, C-8); 169.4 (C, C-10); 178.4 (C, C-2); EIMS *m/z* 451 (M^+) (11), 433 (100), 419 (36), 336 (80), 267 (18), 253 (43), 241 (65), 227 (46), 201 (92); HREIMS calcd for $C_{28}H_{37}NO_4$ 451.2723, found 451.2731; IR (film) ν_{max} 3305, 2926, 2870, 1638, 1589, 1547, 1510, 1440, 1376, 1085, 1022, 869, 755 cm^{-1}.

2.2. Reagents

3-(4,5-dimethylthiazol-2-yl)-2,5-diphenyltetrazolium bromide (MTT) (M5655), adenosine triphosphate (ATP) (A2383), lipopolysaccharide (LPS) from *Escherichia coli* O26:B6 (L2654), MCC950 (PZ0280), nigericin sodium salt (N7143), poly (deoxyadenylic-thymidylic) acid sodium salt (Poly dA:dT) (P0883) and anti-β-Actin−Peroxidase mouse monoclonal antibody (A3854) were purchased from Sigma-Aldrich. Flagellin from *Salmonella typhimurium* (tlrl-stfla), imiquimod (R837), Pam3CysSerLys4 (Pam3CSK4) (tlrl-pms) were obtained from InvivoGen. Disuccinimidyl suberate (DSS) (21555) and trichloroacetic acid (TCA) (10391351) were purchased from ThermoScientific. Lipofectamine® 3000 transfection reagent (L3000008, InvitroGen), Ac-Tyr-Val-Ala-Asp chloromethylketone (Ac-YVAD-CMK) (4018838.0005, Cambridge Bioscience), silica (MIN-U-SIL 15, U.S. Silica). Recombinant Anti-GSDMD antibody (ab209845) and recombinant Anti-pro Caspase-1 + p10 + p12 antibody (ab179515) were purchased from Abcam. Anti-NLRP3/NALP3, mAb (Cryo-2) (AG-20B-0014, Adipogen), mouse IL-1 beta /IL-1F2 antibody (AF-401-NA, R&D Systems), rabbit mAb anti-mouse ASC/TMS1

(D2W8U) (67824S, Cell Signaling Technology). All secondary antibodies were obtained from Agilent, Goat Anti-Rabbit Immunoglobulins/HRP (P044801-2), Rabbit Anti-Goat Immunoglobulins/HRP (P044901-2) and Rabbit Anti-Mouse Immunoglobulins/HRP (P026002-2).

2.3. Isolation and culture of bone marrow-derived macrophages (BMDMs)

Primary bone marrow-derived macrophages (BMDMs) were prepared from tibia and femur of wild-type C57BL/6 mice by centrifuging them in Eppendorf tubes containing phosphate-buffered saline (PBS) at 10,000 × g (15 s). Bone marrow was harvested and red blood cells were lysed. Collected cells were then passed through a cell strainer (70 μm pore) and centrifuged at 1500 x g (5 min). BMDMs were generated by resuspending and culturing the resulting cells in 70% Dulbecco's modified Eagle medium (DMEM) containing 10% (v/v) foetal bovine serum (FBS), 100 U/mL penicillin, and 100 μg/mL streptomycin and supplemented with 30% (v/v) of L929 mouse fibroblast-conditioned media for 7-10 days. Cells were maintained at 37°C, 5% CO_2.

Before experiments, BMDMs were seeded overnight at a density of 1×10^5 cells/well in 96-well plates or 1×10^6 cells/well in 12-well plates in DMEM containing 10% (v/v) FBS, 100 U/mL penicillin, and 100 μg/mL streptomycin.

2.4. Cytotoxicity assay

Cell cytotoxicity was measured by a colorimetric 3-(4,5-dimethylthiazol-2-yl)-2,5-diphenyltetrazolium bromide (MTT) assay, as previously described [47]. Briefly, BMDMs (10^5) were plated in 96-well plates and incubated in the presence of different concentrations of triterpenes for 24 h. MTT was then added and plates were incubated at 37 ºC for additional 3 h. The reaction product, formazan, was extracted with dimethyl sulfoxide (DMSO) and the absorbance was read at 570 nm.

2.5. Inflammasome activation

For induction of canonical NLRP3 inflammasome activation, BMDMs were first primed with 1 μg/mL LPS for 4 h. Then, the medium was replaced with serum-free DMEM and either vehicle (Vh) (DMSO 0.1 %), Caspase-1 inhibitor Ac-YVAD-CMK (YVAD) (100 μM) or triterpenes (at the indicated concentrations) were added for another 30 min. Cells were then treated with one of the following inflammasome activators: nigericin (Nig) (10 μM, 1h), ATP (5mM, 30 min), silica (300 μg/mL, 4h) or imiquimod (IMQ) (75 μM, 1h).

For non-canonical NLRP3 inflammasome activation, BMDMs were primed with 100 ng/mL Pam3CSK4 for 4 h. Cells were then incubated in serum-free DMEM containing either vehicle or triterpenes for 30 min before transfection with 2 μg/mL LPS using Lipofectamine 3000, for 24 h, following the manufacturer's instructions.

For AIM2 and NLRC4 inflammasomes activation, BMDMs were first primed with 1 μg/mL LPS for 4 h. Cells were then incubated in serum-free DMEM containing either vehicle or triterpenes

for 30 min before transfection of the cells with either 1 µg/mL poly (dA:dT) or 1 µg/mL flagellin from *Salmonella typhimurium* for 4 h, respectively using Lipofectamine 3000.

For AIM2 evaluation, cells were pretreated with the NLRP3 inhibitor MCC950 (10 µM) prior to incubation with triterpenes to avoid the possible NLRP3 inflammasome activation triggered by cytosolic DNA as poly (dA:dT) [48, 49].

2.6. Caspase-1 activity assay

Caspase-1 activity was assayed using the bioluminescent method Caspase-Glo 1 inflammasome Assay kit (Promega, G9951) according to the manufacturer's instructions. For the screening of the non-toxic triterpenes, relative luminescence units (RLU) were transformed to percent change, setting 100% for LPS plus nigericin treatment (mean of 4420 ± 903.7 RLU).

2.7. IL-1β measurement

Cell supernatants were collected and IL-1β levels were determined by a mouse IL-1β ELISA kit (Mouse IL-1 β/IL-1F2 DuoSet ELISA, R&D Systems, DY401), according to the manufacturer's instructions. For the screening of the non-toxic triterpenes, IL-1β levels were transformed to percent change, setting 100% for LPS plus nigericin treatment (mean of 1556 ± 372.8 pg/mL).

2.8. Lactate dehydrogenase (LDH) assay

For analysis of pyroptosis, the release of lactate dehydrogenase (LDH) into the cell supernatants was measured by CytoTox 96 Non-Radioactive Cytotoxicity Assay (Promega, G1780), according to the manufacturer's instructions.

2.9. ASC oligomerization assay

BMDMs (10^6) were seeded overnight into 12-well plates. After LPS priming, cells were treated and stimulated as described above. ASC oligomerization was then assayed as previously described [50]. Briefly, BMDMs were lysed directly in-well by using Triton x-100 (1% v/v) and protease inhibitor cocktail, shaking on ice. Total cell lysates were then centrifuged at 6800 x g for 20 min at 4°C to separate the lysate into Triton x-100 soluble and insoluble fractions. The pellet with the insoluble fraction was then chemically crosslinked by addition of disuccinimidyl suberate (DSS, 2 mM, 30 min, RT) in PBS. After crosslinking, the insoluble fraction was spun at 6800 x g for 20 min and the resulting pellet was resuspended and boiled in 40 µL of Laemmli buffer (1X). Western blot analysis was then performed.

2.10. Western blot analysis

The Triton x-100 soluble fraction (containing cell lysates) was concentrated by trichloroacetic acid (TCA) precipitation, washed in acetone, and spun for 10 min at 14,000 x g at 4°C. The pellet obtained was allowed to air dry before resuspending in 2X Laemmli buffer. Then, samples were separated by SDS-PAGE and transferred onto PVDF membranes using a Trans-Blot Turbo system (Bio-Rad). Membranes were blocked for 1 h at room temperature (RT) in 5% w/v milk in PBS containing 0.1% Tween 20 (PBS-T) before incubation (overnight, 4°C) with indicated primary antibodies in bovine serum albumin (5% w/v) in PBS-T. Membranes were washed before

incubation (1 h, RT) with appropriate HRP-conjugated secondary antibodies. For proteins visualization, membranes were incubated with Amhersam ECL prime western blotting detection reagent (Cytiva, RPN2236) and chemiluminescence was visualized using a G:Box Chemi XX6 (Syngene). β-Actin was used as a loading control. All the antibodies used are reported in section 2.2.

2.11. Protein preparation and molecular docking

Docking studies were performed using Glide v9.1 The structure of NLRP3 (PDB 7ALV) was prepared for docking using the Protein Preparation Workflow (Schrodinger, LLC, New York, NY, USA, 2021) accessible from the Maestro program (Maestro, version 12.8; Schrodinger, LLC: New York, NY, USA, 2021). Bond corrections were applied to the cocrystallized ligand and an exhaustive sampling of the orientations of groups was performed. Finally, the receptor was optimized in Maestro 12.8 by using OPLS4 force field before docking study. In the final stage the optimization and minimization on the ligand-protein complexes were performed and the default value for RMSD of 0.30 Å for non-hydrogen atoms were used. The receptor grids were generated using the prepared protein, with the docking grids centered at the bound ligand. The ADP binding site was enclosed in a grid box of 20 $Å^3$ without constrains. The three-dimensional structures of the ligand to be docked were generated and prepared using LigPrep as implemented in Maestro 12.8 (LigPrep, Schrodinger, LLC: New York, NY, USA, 202**1**) to generate the most probable ionization states at pH 7 ± 1 (retaining the original ionization state). Finally, the geometries were optimized using OPLS4 force field. These conformations were used as the initial input structures for the docking. The ligand was docked using the extra precision mode (XP) [51]. The dockings were carried out with flexibility of the residues of the binding site near to the ligand. The generated ligand poses were evaluated with empirical scoring function implemented in Glide [52].The XP Pose Rank was used to select the best-docked pose for each ligand.

2.12. Covalent docking

Covalent docking studies were performed using the module CovDock workflow as implemented in Schrödinger Suite 2021–2 version. The CovDock workflow has been reported to be highly accurate in pose prediction of covalent inhibitors [53]. The prepared ligands were selected from project table and were confined to the box, which was the centroid of ADP. The enclosing box size was calculated automatically based on the size of ADP. The residue Cys 415 was defined as reactive residue from crystal structure of NLRP3 NACHT (PDB 7ALV) domain in complex with an inhibitor on the workspace. The customized covalent docking algorithm was then selected as the reaction type. No constraints were imposed on the ligand for docking and pose prediction mode was selected. The total energy 2.5 kcal/mol was set as the cutoff to retain poses for further refinement by default, while the maximum number of poses to retain for further refinement, was 200. The output poses per ligand reaction site was set to 10 best poses, also the scoring option

MM-GBSA was selected in order to obtain more information about the binding affinity of the poses and the best scoring poses were analyzed.

2.13. Statistical analysis

All data are presented as means ± S.D. for at least three independent experiments together with individual data points where possible. Statistical significance was estimated by one-way ANOVA with Dunnett's post-hoc test and differences were considered significant at $p < 0.05$. All statistical analyses and estimated values of the half-maximal (50%) inhibitory concentration (IC_{50}) and the half-maximal (50%) effective concentration (EC_{50}) were conducted using GraphPad Prism Software 9 (CA, USA).

3. RESULTS AND DISCUSSION

3.1. Chemistry

Triterpenes (**1-11)** were isolated from the roots of *Maytenus retusa* (Celastraceae) (Fig. 1) [46].

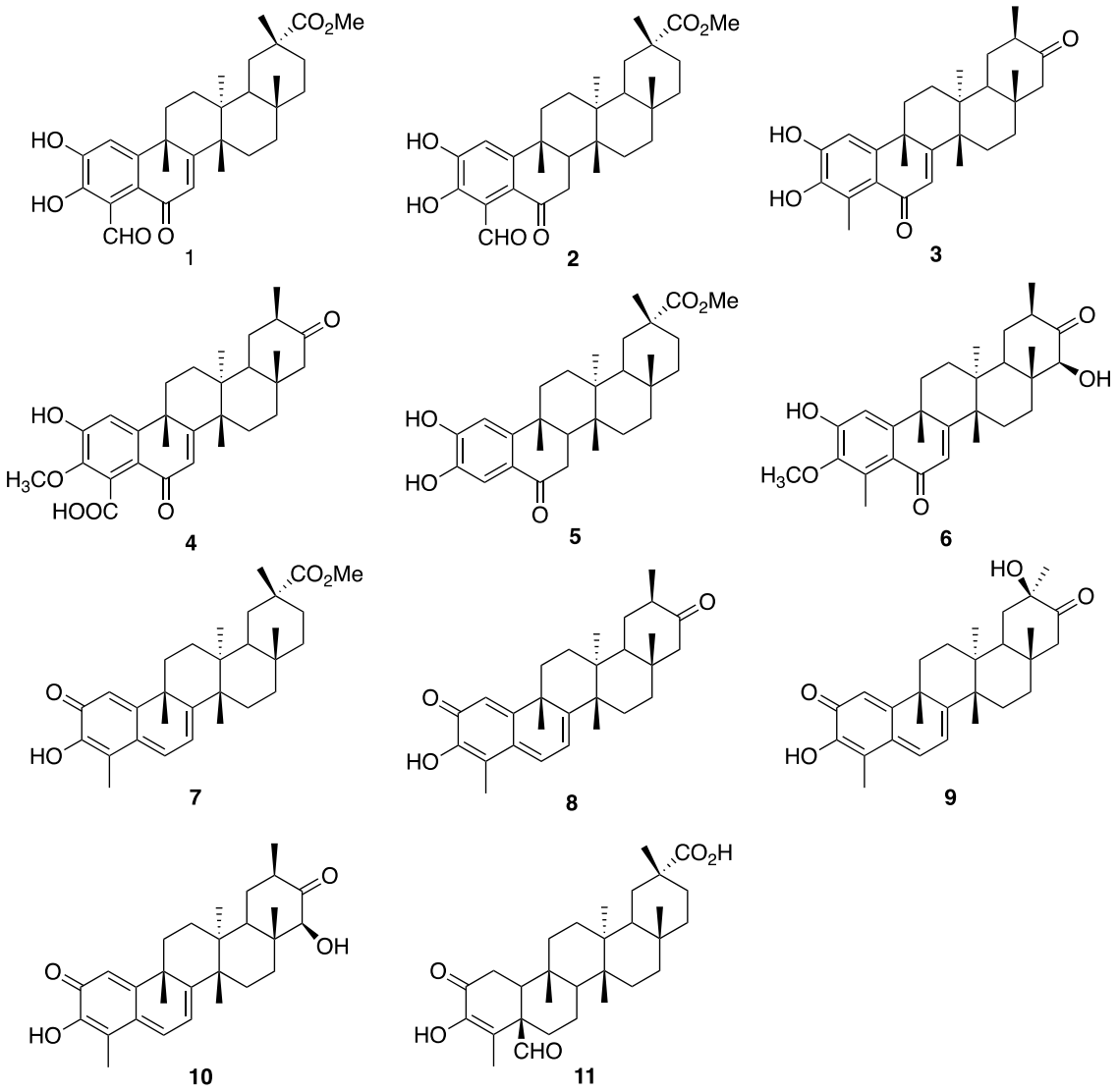

Figure 1. Structures of triterpenes (**1**-**11**)

Derivatives (**12**-**16**) were obtained from tingenone (**8**) and 22-β-hydroxy-tingenone (**10**) as it is shown in Scheme 1. Thus, the treatment of compound **10** with BBr_3 yielded the brominated compound (**12**) together with compound **13** in 27% and 40% yield, respectively. When **8** was reacted with NBS the derivative **14** with a bromine at C-11 was obtained. Finally, the reaction of the triterpenequinones **8** and **10** with hydroxylamine hydrochloride afforded the corresponding oximes **15** and **16**, respectively.

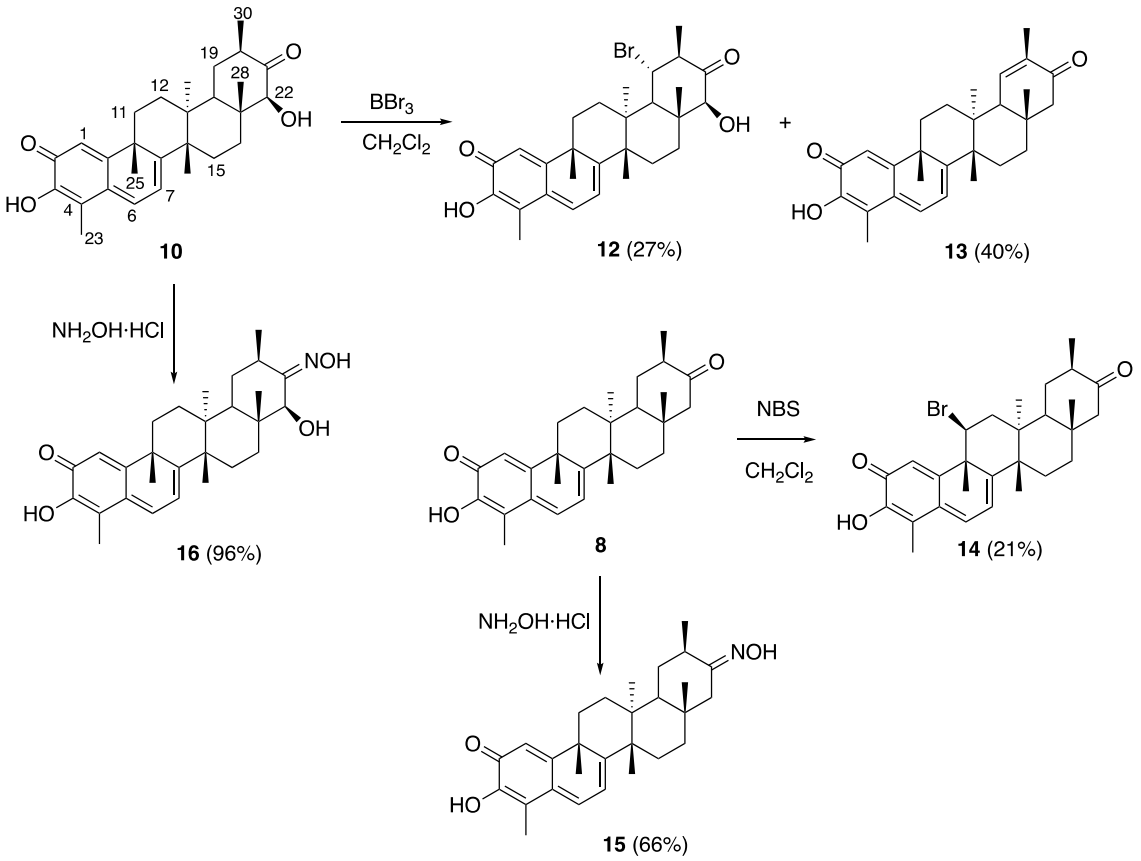

Scheme 1. Preparation of derivatives (**12-16**)

3.2. Cytotoxicity evaluation

To assess the potential cytotoxicity of triterpenes (**1-16**), cell viability was tested in BMDMs treated with compounds at the range of 0.25-20 μM using the MTT assay. Cell viability in presence of the compounds is shown in Fig. 2. and the estimated values for the half-maximal effective concentration (EC_{50}) are reported in Table 1.

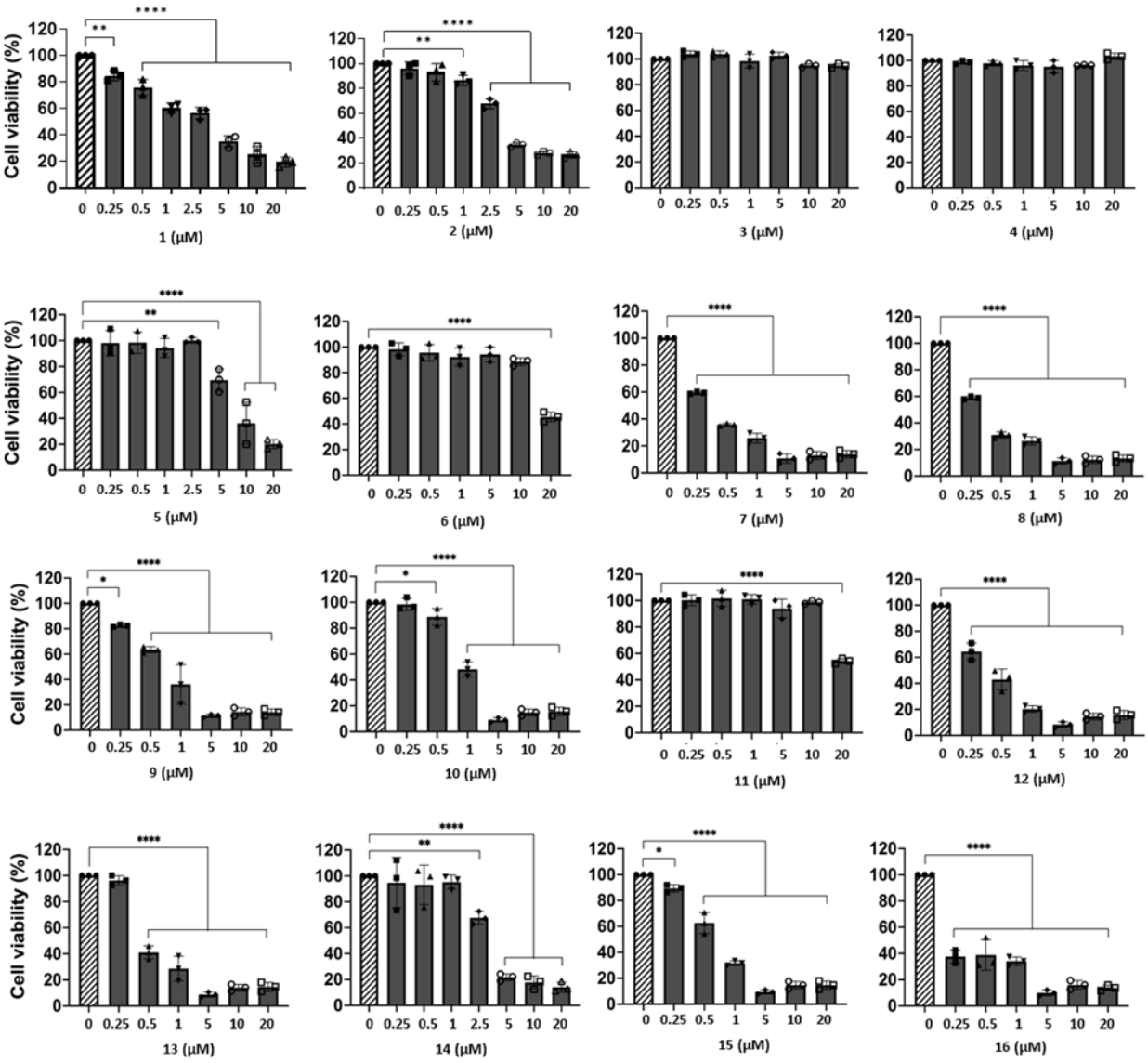

Figure 2. Cytotoxic effects of triterpenes (1-16) in BMDMs. Cell viability after treatment with derivatives 1-16 (0 - 20 μM) for 24 h was determined by MTT assay. Results are reported as mean ± SD (n = 3). *p < 0.05, **p < 0.01, ***p < 0.001 and ****p < 0.0001 *vs*. untreated cells.

Triterpene	1	2	3	4	5	6	7	8	9	10	11	12	13	14	15	16
EC_{50} (μM)	2.45	2.7	>20	>20	7.1	18.7	0.29	0.26	0.79	1.2	>20	0.28	0.54	2.94	0.7	<0.25

Table 1. Estimated EC_{50} values for cytotoxic effects of triterpenes (**1-16**) in BMDMs.

Compounds **1**, **7**, **8**, **9**, **10**, **12**, **13**, **15** and **16** exhibited high cytotoxicity and were therefore not selected for further evaluation. By contrast, derivatives **2**, **3**, **4**, **5**, **6, 11** and **14** did not reduce cell viability significantly in the concentration range of 0.25–1 μM, as cell viability was maintained over 80%. Since these compounds were not cytotoxic to BMDMs at low concentrations, they were selected for further studies at sub-cytotoxic concentrations.

From a structural point of view, all triterpenequinones, except **14,** with a bromine at C-11 were cytotoxic, while the triterpene cangoronin (**11**) and almost all *nor*-triterpene phenols were not cytotoxic. Among them, only zeylasteral (**1**) having a formyl group at C-4 and a double bond at C7-C8 was toxic. The presence of both functional groups in the nor-triterpene phenol series produces cytotoxicity since macrocarpin a (**2**), with identical structure of (**1**) except the presence of the double bond, was not cytotoxic.

3.3. Effects of triterpenes on NLRP3 inflammasome activation

The cleavage of caspase-1 is an essential step in the release of pro-inflammatory cytokine IL-1β and pyroptotic cell death after NLRP3 inflammasome activation. Active caspase-1 cleaves pro-IL-1β to the mature cytokine IL-1β which is then released from the cell to enhance inflammatory responses. To test the potential effects of the selected triterpenes **2**, **3**, **4**, **5**, **6**, **11** and **14** on canonical NLRP3 inflammasome activation, LPS-primed BMDMs were treated with the selected triterpenes at the indicated non-cytotoxic concentrations, and were then stimulated with nigericin to cause NLRP3 inflammasome activation. Nigericin is a potassium ionophore that directly mediates K^+ efflux through forming pores in the membrane, subsequently activating NLRP3 inflammasome by the canonical pathway [54]. Caspase-1 activity and subsequent IL-1β release were then measured (Fig. 3A,B).

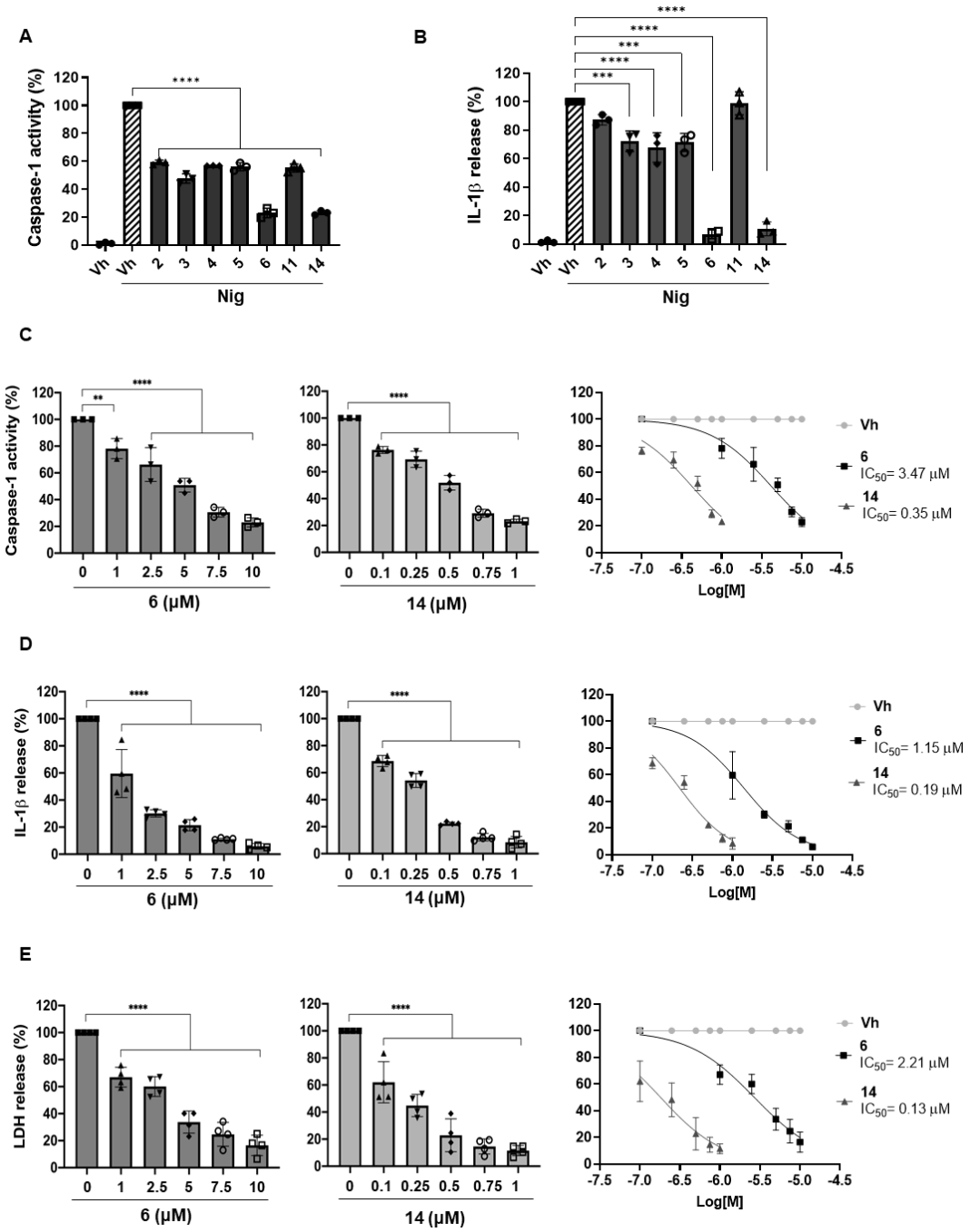

Figure 3. Triterpene derivatives inhibit NLRP3 inflammasome activation in BMDMs. (A,B) LPS-primed (1 μg/mL, 4 h) BMDMs were preincubated with triterpenes at the maximum non-cytotoxic concentration (**2**, 1 μM; **3**, 20 μM; **4**, 20 μM; **5**, 2.5 μM; **6**, 10 μM; **11**, 10 μM; **14**, 1 μM) for 30 min prior to nigericin (Nig) activation (10 μM, 1 h) or vehicle (Vh) treatment. (A) Caspase-1 activity was then assayed using Casp-Glo 1 kit and expressed as percentage of relative luminescence units. (B) IL-1β released into the culture medium was measured by ELISA and expressed as percentage of IL-1β levels. (C, D, E) LPS-primed BMDMs were preincubated with the indicated dose of **6** (1 - 10 μM) or **14** (0.1 - 1 μM) for 30 min prior to Nig activation (10 μM, 1h). (C) Dose-dependent effects of **6** and **14** on caspase-1 activity. (D) Dose-dependent effects

of **6** and **14** on IL-1β release. (E) Dose-dependent effects of **6** and **14** on pyroptotic cell death. LDH release was measured in the culture supernatants by the CytoTox® kit. All the results were normalized to Nig condition and reported as mean ± SD of at least 3 independent experiments. **p < 0.01, ***p < 0.001 and ****p < 0.0001 *vs*. LPS + Nig.

All triterpenes exhibited discernible inhibitory effects, with a significant reduction of caspase-1 activity when compared to cells treated with LPS and nigericin (Fig. 3A). Pretreatment of the primed cells with triterpenes **3**, **4**, **5**, **6** and **14** also significantly reduced IL-1β release (Fig. 3B). As observed, triterpenes **6** and **14** were the most active compounds in both assays, managing to reduce both caspase-1 activity and IL-1β secretion by more than 50% compared to the LPS plus nigericin condition. Therefore, they were selected for further evaluation. LPS-primed BMDMs were pretreated with various doses of triterpene **6** (1-10 µM) or triterpene **14** (0.1-1 µM), and then stimulated with the NLRP3 activator nigericin. As shown in Fig. 3C, compounds **6** and **14** inhibited caspase-1 activity in a concentration dependent-manner with IC_{50} values of 3.47 and 0.35 µM, respectively. They also dose-dependently reduced IL-1β released into cell supernatants in the same treatment conditions, with IC_{50} of 1.15 and 0.19 µM, respectively (Fig. 3D).

The influence of substitution patterns of the phenolic nor-triterpenes on their inhibitory activity was analyzed. Considering the phenolic ring, the extended B-ring conjugation and the E-ring substitution, the obtained results indicated that the most effective group at C-4 was a methyl group (**4** vs **6**). The presence of a conjugated double bond at C-7-C-8 and the existence of a carbonyl group at C-21 are also important since both are present in the most active compound **6** Furthermore, an additional hydroxy group at C-22 seems to increase the inhibitory activity (**6** vs **3**).

Active caspase-1 also cleaves GSDMD, which forms pores in the membrane leading to the inflammatory-induced cell death pyroptosis, which can be measured by LDH release. We next examined whether compounds **6** and **14** affected pyroptosis during activation of NLRP3 inflammasome. Treatment with nigericin after LPS priming enhanced LDH release, which was significantly reduced by compounds **6** and **14** in a dose-dependent manner with IC_{50} values of 2.21 and 0.13 µM, respectively (Fig. 3E). These data indicated that both triterpenes suppressed caspase-1 mediated pyroptosis.

Interestingly, pyroptosis is described as an important mechanism involved in the pathogenesis of many diseases including cardiovascular, metabolic and neurodegenerative diseases, and cancer [55-57]. Therefore, agents as **6** and **14** with the ability of suppress this type of cell death, could be promising therapeutic agents.

Taking these results together suggested that triterpenes **6** and **14** could efficiently inhibit NLRP3 inflammasome activation in LPS-primed murine macrophages upon canonical stimulation with nigericin.

NLRP3 is activated in response to many diverse stimuli, with K^+ efflux reported as one of the main intracellular events involved in its activation. Aside from nigericin, extracellular ATP and particulate matter, such as silica crystals, are other commonly used agonists for canonical NLRP3 inflammasome activation. Both activators act via a K^+ efflux-dependent mechanism. ATP as a ligand of the purinergic receptor P2X7 [58] and silica crystals causing lysosomal disruption [14]. To further confirm the inhibitory potential of compounds **6** and **14** on NLRP3 inflammasome, we next investigated their activity after stimulation with these other NLRP3 agonists. LPS-primed BMDMs were pretreated with triterpene **6** (5, 10 μM) or **14** (0.5, 1 μM) followed by activation with either extracellular ATP, or silica crystals. Supernatants were then analysed for IL-1β and LDH release (Fig. 4).

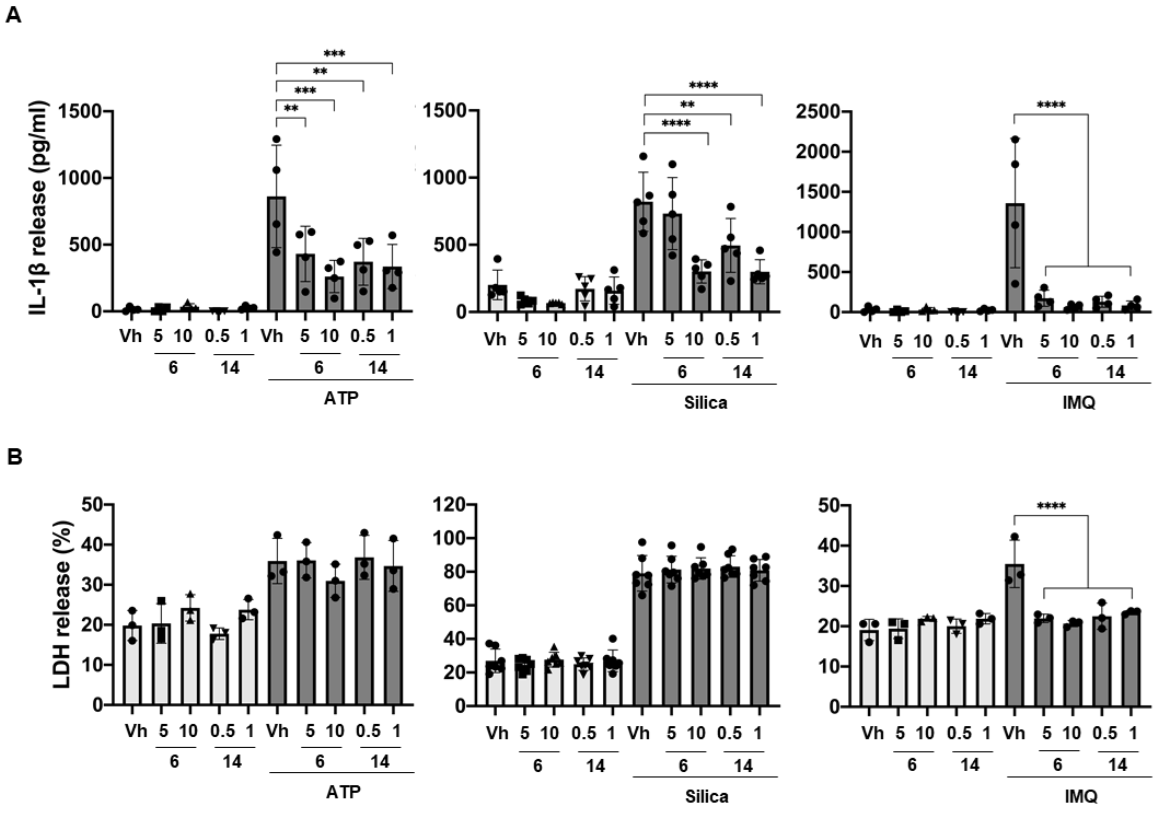

Figure 4. Triterpenes 6 and 14 inhibit NLRP3 inflammasome activation triggered by other stimuli. LPS-primed (1 μg/mL, 4 h) BMDMs were preincubated with triterpenes **6** (5, 10 μM), **14** (0.5, 1 μM) or Vh control for 30 min. Then, NLRP3 activator was added (ATP 5 mM, 30 min; Silica 300 μg/mL, 4 h or imiquimod (IMQ) 75 μM, 1h). (A) IL-1β released into the culture

supernatants was measured by ELISA. (B) Pyroptotic cell death was assayed by measuring LDH release in the culture supernatants by the CytoTox® kit and expressed as percentage of total LDH. Results were reported as mean ± SD of at least 3 independent experiments. **$p < 0.01$, ***$p < 0.001$ and ****$p < 0.0001$ *vs*. LPS + stimuli treatment.

Both triterpenes significantly inhibited IL-1β production induced by ATP and silica stimuli. However, they had no significant effects on pyroptotic cell death, measured in terms of LDH release when these activators were used (Fig. 4 A,B).

To better understand the mechanism of NLRP3 inhibition exerted by these compounds, LPS-primed BMDMs were pretreated with the triterpenes followed by activation with imiquimod (IMQ). Imiquimod is a mitochondrial disruptor that induces ROS formation, thus leading to canonical NLRP3 inflammasome activation, independently of K^+ efflux [15]. In response to IMQ, IL-1β and LDH release were potently inhibited by triterpenes **6** and **14** (Fig. 4 A,B).

Collectively, these results not only suggest that compounds **6** and **14** potently inhibited the activation of the NLPR3 inflammasome triggered by broad proinflammatory activators, but also that their inhibitory activity did not depend on K^+ efflux, suggesting that both triterpenes might act downstream of this signaling event.

Therefore, we next tested whether the regulation of the NLRP3 inflammasome response carried out by both triterpenes was due to a direct caspase-1 enzyme inhibition. For this purpose, BMDMs were primed with LPS followed by nigericin stimulation to activate caspase-1. Following pyroptosis, caspase-1 activity can be detected in the supernatant. Therefore, cell-free supernatants were collected and then incubated with either **6**, **14** or the caspase-1 inhibitor Ac-YVAD-CFK (YVAD) and assayed for caspase-1 activity. As shown in Fig. 5, nigericin treatment increased caspase-1 activity, which was completely inhibited after YVAD treatment. Neither compound **6** nor **14** directly affected active caspase-1 specifically, indicating that they might directly target the NLRP3 inflammasome complex assembly.

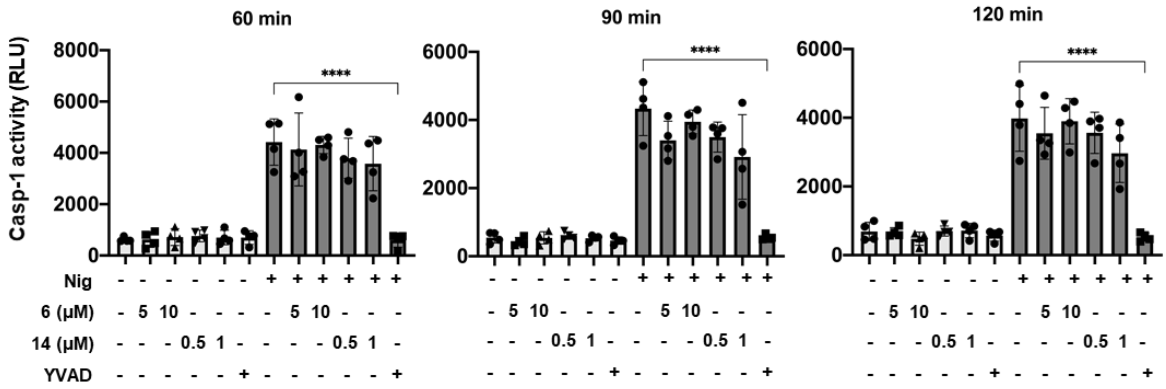

Figure 5. Compounds 6 and 14 do not specifically target caspase-1. LPS-primed (1 μg/mL, 4 h) BMDMs were stimulated with Nig (10 μM) for 1 h. After caspase-1 activation, culture supernatants were collected and incubated with either triterpenes **6** (5, 10 μM), **14** (0.5, 1 μM), caspase-1 inhibitor Ac-YVAD-CMK (YVAD) (100 μM) or Vh for 15 min. Caspase-1 activity was then measured in these supernatants after 60, 90 and 120 min, using the Casp-Glo 1 kit. Results were reported as mean ± SD of relative luminescence units (RLU) (n = 4). ****$p < 0.0001$ *vs*. LPS + Nig treatment.

3.5. Triterpenes 6 and 14 blocked ASC oligomerization

ASC oligomerization is a key step during NLRP3 inflammasome activation leading to NLRP3 assembly and subsequent caspase-1 activation [5, 59]. Thus, the effects of triterpenes **6** and **14** on this process were evaluated. LPS-primed BMDMs treatment with triterpenes remarkably suppressed nigericin-induced ASC oligomerization, as indicated by a reduction in ASC oligomers (Fig. 6). As expected, the subsequent levels of cleaved IL-1β (cIL-1β), the active subunit of caspase-1 (Casp-1 p10) and the cleaved GSDMD fragment (GSDMD-N) were also reduced in response to treatment with both compounds. The expression of the precursor components was unaffected (GSDMD, Casp-1 p45 and pro-IL-1β).

Together, these results suggested that both compounds suppressed the oligomerization of the adaptor protein ASC, thus disrupting inflammasome complex assembly and inhibiting the subsequent caspase-1 activation, IL-1β production and pyroptosis.

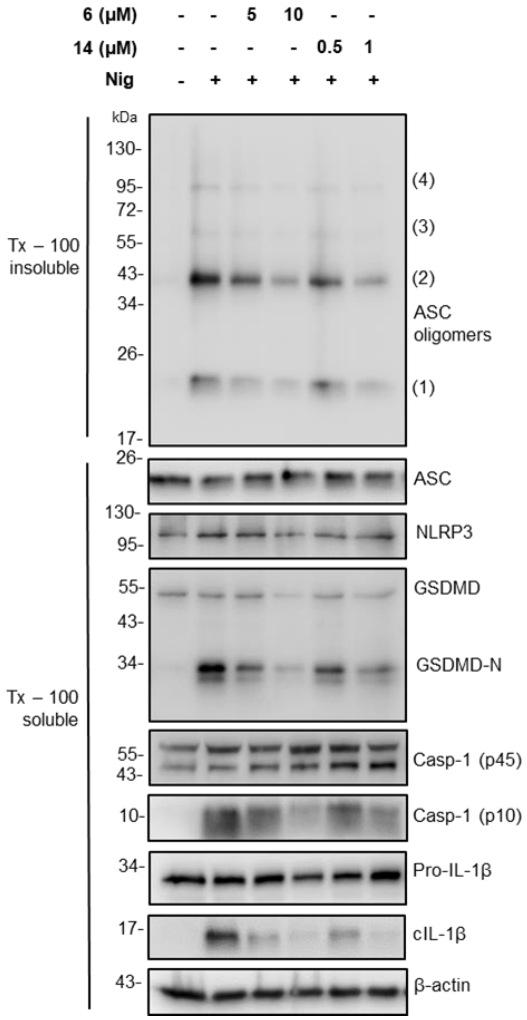

Figure 6. Triterpenes 6 and 14 block ASC oligomerization. LPS-primed (1 μg/mL, 4 h) BMDMs were preincubated with **6** (5, 10 μM) or **14** (0.5, 1 μM) for 30 min before Nig stimulation (10 μM, 1 h). Western blot analysis of Triton x-100 insoluble crosslinked ASC oligomers and soluble total BMDMs cell lysates probed for ASC, NLRP3, GSDMD, caspase-1, IL-1β and β-actin as a loading control (n = 4).

3.6. Triterpenes 6 and 14 affected non-canonical NLRP3 activation

In the non-canonical pathway, intracellular LPS from Gram-negative bacteria can activate the NLRP3 inflammasome through a caspase-11 dependent mechanism [60]. After sensing cytosolic

LPS (cLPS), caspase-11 cleaves GSDMD, which forms pores in the membrane inducing pyroptosis and K+ efflux, which in turns activates the NLRP3 inflammasome.

The effect of the triterpenes **6** and **14** on non-canonical NLRP3 activation pathway was also evaluated. After priming BMDMs with the TLR2/TLR1 ligand Pam3CSK4 for 4 hours, cells were treated with the triterpenes before LPS transfection to activate the non-canonical pathway. Both compounds significantly reduced IL-1β production at the highest dose used, thus impairing this pathway (Fig. 7). Interestingly, triterpenes **6** and **14** could not block cLPS-induced pyroptosis, suggesting that they target downstream of caspase-11 to inhibit non-canonical NLRP3 activation. Thus reinforcing our findings that **6** and **14** act through the disruption of NLRP3 inflammasome assembly.

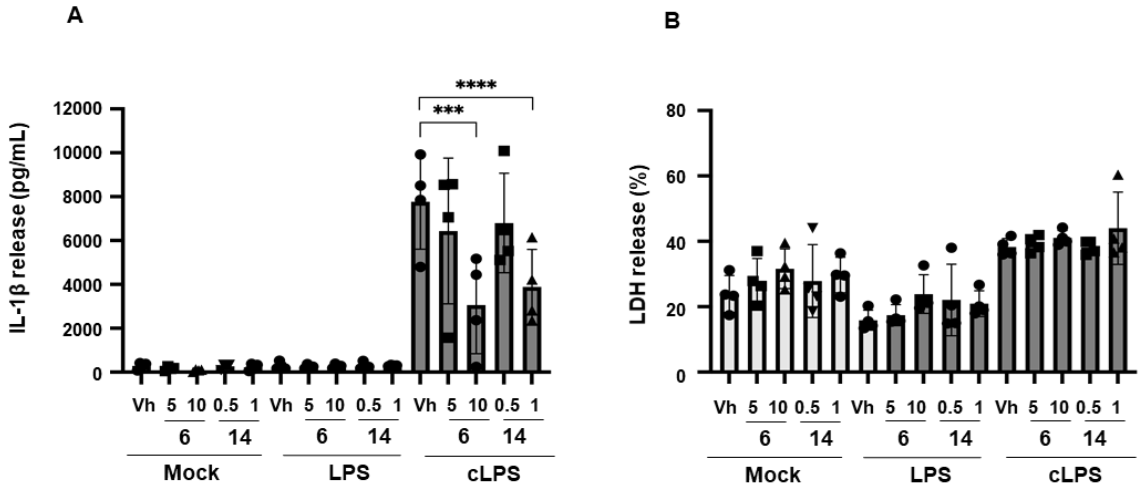

Figure 7. Triterpenes 6 and 14 also affect non-canonical NLRP3 activation. BMDMs were firstly primed with 100 ng/mL Pam3CSK4 for 4 h followed by preincubation with triterpenes **6** (5, 10 µM), **14** (0.5, 1 µM) or Vh control for 30 min. Then, cells were stimulated with 2 µg/mL of cytosolic LPS (cLPS) for 24 h. (A) IL-1β levels in cell supernatants were measured by ELISA. (B) Pyroptotic cell death was assayed by measuring LDH release in the culture supernatants by the CytoTox® kit and expressed as percentage of total LDH. Results are reported as mean ± SD (n = 4). ***p < 0.001 and ****p < 0.0001 *vs*. Pam3CSK4 + cLPS.

3.7. Triterpenes 6 and 14 had no effects on AIM2 and NLRC4 inflammasomes

NLRP3 is the most clinically implicated inflammasome, playing key roles in many chronic inflammatory and autoimmune human diseases. On the contrary, other inflammasomes such as AIM2 and NLRC4 have been mainly associated with acute immune responses against pathogens. We finally investigated the potential effects of triterpenes **6** and **14** on other inflammasomes (AIM2 and NLRC4). To this end, LPS-primed BMDMs were either transfected with double-

stranded DNA poly (dA:dT) (1 µg/mL) to activate the AIM2 inflammasome or flagellin from *S. typhimurium* (1 µg/mL) to activate the NLRC4 inflammasome. Pretreatment with triterpenes **6** or **14** did not affect IL-1β or LDH release induced by AIM2 or NLRC4 activation (Fig. 8A, B).

The above data strongly suggest that triterpenes **6** and **14** act specifically as NLRP3 inhibitors, indicating that its use could reduce off-target immunosuppressive effects.

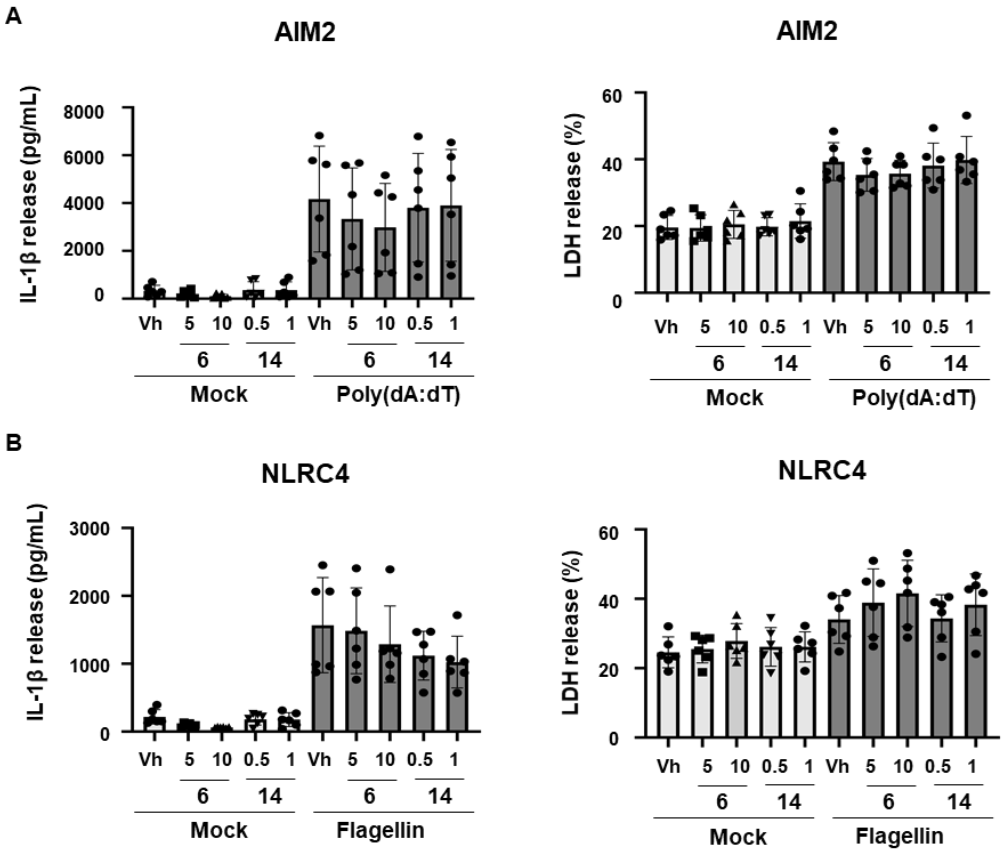

Figure 8. Triterpene derivatives 6 and 14 do not affect AIM2 and NLRC4 inflammasomes activation. LPS-primed (1 µg/mL, 4 h) BMDMs were preincubated with triterpenes **6** (5, 10 µM), **14** (0.5, 1 µM) or Vh control for 30 min and then stimulated with 1 µg/mL cytosolic poly(dA:dT) (A) or 1 µg/mL flagellin (B) for 4 h. IL-1β and LDH release were then measured in cell supernatants. Results are reported as mean ± SD (n = 6).

3.8. Covalent Docking Studies on NLRP3

The general mechanism for the inhibition of an enzyme or receptor by a small molecule drug is that the drug binds to the protein, inhibiting its activity through non-covalent interactions, such as hydrogen bonds, hydrophobic, or π-π-stacking interactions, among others. So these binding

energies are sufficiently weak for the binding to be reversible. Nevertheless, covalent inhibition of therapeutic protein targets has gained increasing interest in the last two decades [61, 62]. About 30% of marketed drugs that target enzymes act as covalent inhibitors [63] which retain significant advantages over noncovalent inhibitors and result in highly selective inhibition [64]. Covalent bonds are generally formed by the interaction between a reactive functional group on the ligand and a nucleophilic residue such as cysteine, leading to the formation of covalent adducts [65]. The improvement of selective irreversible covalent inhibitors has been the focus of much research on positive health effects [64].

Hence, conventional (non-covalent) and covalent docking studies of the active compounds were carried out using the Glide software [66] on the reported crystal structure of NLRP3 in complex with the potent inhibitor MCC950 analog (PDB 7ALV), in order to propose a plausible mechanism of action, as well as to understand the binding mode and key interactions at the active site that drive inhibition of NLRP3 inflammasome activation. NLRP3 is composed of a central triple-ATPase domain called NACHT that mediates protein oligomerization upon activation [12]. Likewise a set of conserved cysteines present in the NACHT domain are important for inflammasome activation [67]. In distressed or damaged tissues extracellular ATP concentrations rise. Therefore, the ATPase activity within the NACHT domain needs to cleave ATP into ADP in order to achieve the active conformation, leading to NEK7 protein recruitment and subsequent inflammasome complex oligomerization and assembly [68]. Whatever stimulus triggers NLRP3 inflammasome activation, conformational changes are required in the switch from the inactive resting conformation to the active structure. All of this suggests that blocking ATPase activity is a feasible strategy with which to target the design of compounds that can inhibit the syndromes associated with inflammatory disorders.

A deeper analysis of the non-covalent docking result showed that the best docking scores for the active compounds were found in the range from -4.30 to 3.57 kcal·mol^{-1}. These results strongly suggested that the binding site of the potent inhibitor MCC950 analog is not the same as for the two most active compounds, since, as can be seen, they present considerably low binding affinity values. Likewise, the binding modes of the compounds studied could not be correctly predicted and a correlation could not be achieved between the score values obtained and the biological activity values. Furthermore, no type of hydrogen bond interaction is observed that could be key to the affinity with the receptor, suggesting that the hydrophobic interactions present are not so effective in providing a stabilizing effect to the protein-ligand complex formed.

In accordance with the above and taking into consideration the structural features of the most active compounds **6** and **14**, the presence of an α, β- unsaturated carbonyl moiety in its structures that could act as a Michael acceptor can be observed. Therefore, covalent docking was performed at the ATP binding site, since Michael acceptors are able to react with biological nucleophilic

residues, such as cysteine and thus form covalent bonds. These observations allowed us to hypothesize that the NLRP3 inflammasome could be a sensitive target to be inhibited by the compounds under study.

Thus, it can be seen how the compound **14** fits well within the ATP binding site of the inflammasome, occupying a large portion of it. (Fig. 9).

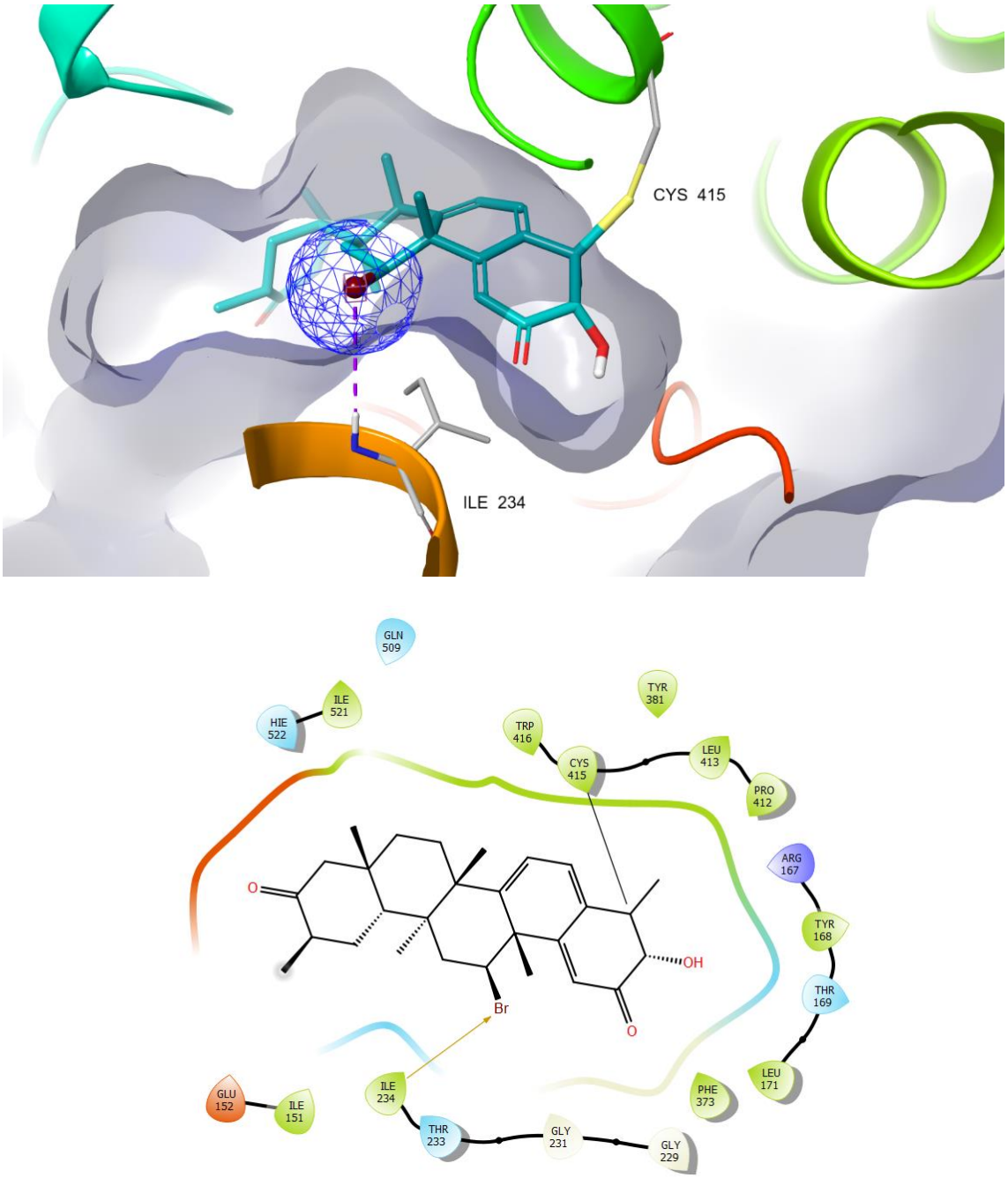

Figure 9. Covalent docking of compound **14** into the ADP binding site (PDB 7ALV) and its key interactions.

As we expected, the docking result suggested that the compound **14** could bind covalently to NLRP3, forming a covalent bond between Cys415 and the β carbon of the α, β unsaturated

carbonyl moiety. In addition, another important aspect that can be derived from the predicted pose of compound **14** is the ability to also form a halogen bond interaction, between the bromine present in the structure and a residue of Ile 234. Halogen bonds (or X-bonds) has recently been recognized as short-range electrostatic interactions that play an important role in affinity control and recognition of inhibitors against their therapeutic targets [69]. Furthermore, multiple potential hydrophobic interactions involving residues such as Ile 151, Glu 152, Gly231, Gly 229, Ile 234, Phe 373, Tyr381, Leu 413, Trp416, Pro 412, Gln509, Ile 521.

Additionally, these results showed a considerable increase in the score value for the most stable conformation when compared with the scores obtained from the analysis of the non-covalent docking results. According to the predicted binding mode, the cdock affinity values calculated for the compound **14** were found in the range from −7.48 to −8.11 kcal mol^{-1}, suggesting these interactions were so effective that they provided a stabilizing effect on the active site conformation.

On the other hand, further analysis of the results of the predicted pose of compound **6** obtained by covalent docking revealed that this active compound may be capable of covalently binding to the residue of Cys 415 forming a tetrahedral intermediate, which is obtained as a result of a nucleophilic attack on the carbonyl group of the structure (Fig. 10). This unexpected nucleophilic addition on an α, β-unsaturated carbonyl moiety can be explained by the steric hindrance produced by the two methyl groups close to the double bond that are in beta configuration, preventing the formation of the covalent bond. In addition, the formation of a hydrogen bond between the hydroxyl group of ring E and a residue of Glu152 can also be observed. The cdock affinity value calculated for this compound was −8.06 kcal mol^{-1}. Multiple hydrophobic interactions similar to those observed with compound **14** since both occupy the same region in the ATP binding site were also detected.

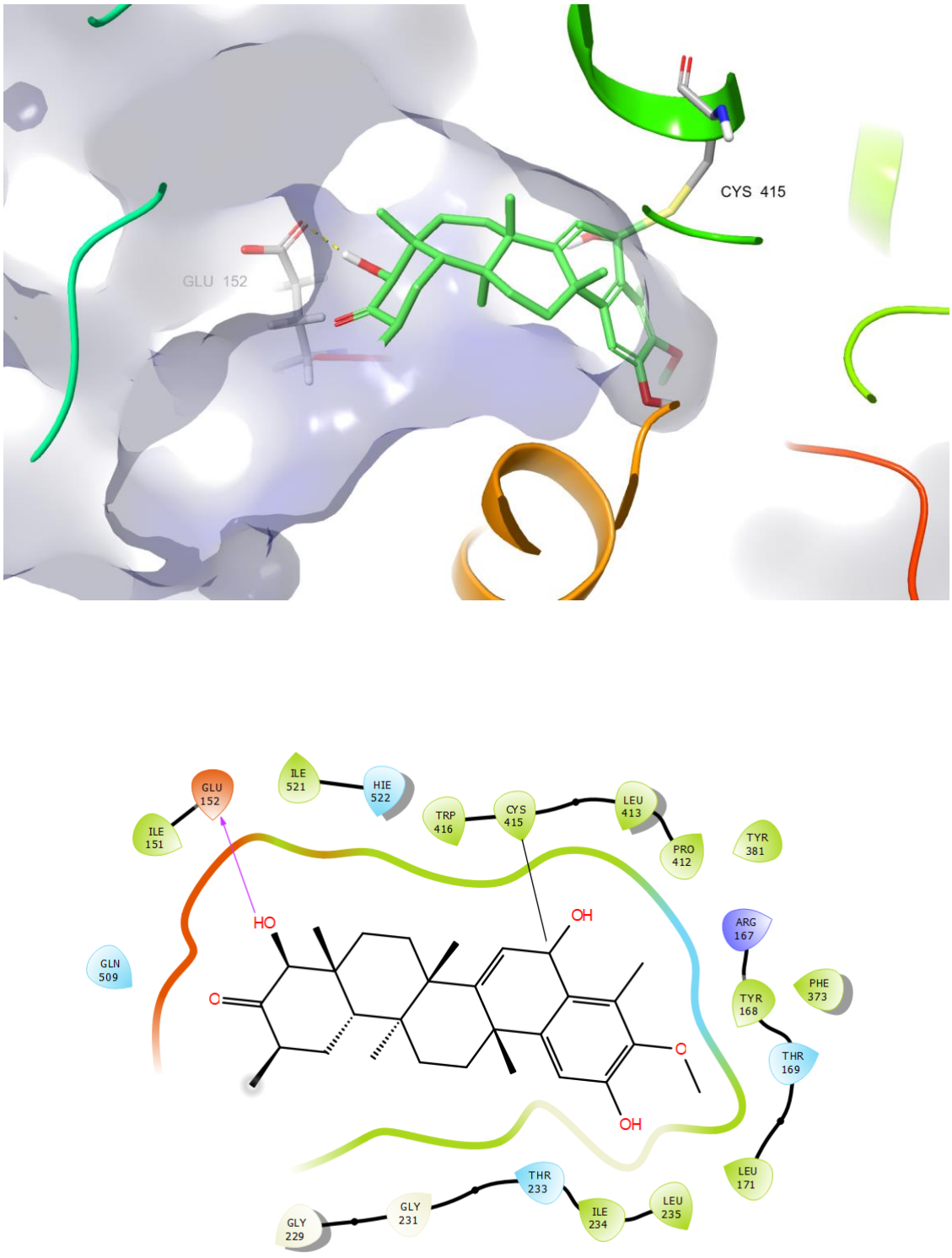

Figure 10. Covalent docking of compound **6** into the ADP binding site (PDB 7ALV) and its key interactions.

In conclusion, our analysis has revealed that compound **6** and compound **14** may form covalent bonds with a cysteine residue in the NACHT domain, thereby potentially blocking the interaction between NLRP3 and NEK7, preventing a conformational change and avoiding the assembly and activation of the NLRP3 inflammasome through the inhibition of its ATPase activity.

4. Conclusion

In this study, the effects of a series of phenolic and quinone methide *nor*-triterpenes isolated from *Maytenus retusa* and some semisynthetic derivatives on inhibition of NLRP3 inflammasome activation were examined. The phenolic *nor*-triterpene (**6**) and the semisynthetic *nor*-triterpenequinone (**14**) resulted be potent inhibitors of both canonical and non-canonical NLRP3 inflammasome activation. Mechanistically, these compounds blocked inflammasome assembly independently of K^+ efflux, leading to a reduction of IL-1β and pyroptotic cell death. Nevertheless, they had no inhibitory effects on the NLRC4 and AIM2 inflammasomes. Collectively, these results strongly encourage further evaluation of both triterpenes as promising therapeutic agents for NLRP3-related inflammatory diseases. Moreover, they could serve as lead compounds in the development of new selective NLRP3 inflammasome inhibitors.

Declaration of Competing Interest

The authors declare that they have no known competing financial interests or personal relationships that could have appeared to influence the work reported in this paper.

Funding

This study was supported by Instituto de Salud Carlos III (PI17CIII/00012, PI20CIII/00018); Spanish Ministry of Science, Innovation and Universities (RTI2018-094356-B-C21) and Agencia Canaria de Investigación, Innovación y Sociedad de la Información (Pro ID 2021010037). LGC received a predoctoral fellowship award and a complementary mobility grant from the Spanish Ministry of Universities (FPU17/03519, EST22/00224). AA and SOR thanks to Cabildo de Tenerife (Agustín de Bethancourt Program).

REFERENCES

[1] F. Martinon, A. Mayor, J. Tschopp, The inflammasomes: guardians of the body, Annu. Rev. Immunol 27 (2009) 229-65.

[2] B.K. Davis, H. Wen, J.P. Ting, The inflammasome NLRs in immunity, inflammation, and associated diseases, Annu Rev Immunol 29 (2011) 707-35.

[3] P. Broz, V.M. Dixit, Inflammasomes: mechanism of assembly, regulation and signalling, Nat. Rev. Immunol 16(7) (2016) 407-20.

[4] M. Groslambert, B.F. Py, Spotlight on the NLRP3 inflammasome pathway, J Inflamm Res 11 (2018) 359-374.

[5] F. Hoss, J.F. Rodriguez-Alcazar, E. Latz, Assembly and regulation of ASC specks, Cell Mol Life Sci 74(7) (2017) 1211-1229.
[6] W.T. He, H. Wan, L. Hu, P. Chen, X. Wang, Z. Huang, Z.H. Yang, C.Q. Zhong, J. Han, Gasdermin D is an executor of pyroptosis and required for interleukin-1beta secretion, Cell Res 25(12) (2015) 1285-98.
[7] X. Liu, Z. Zhang, J. Ruan, Y. Pan, V.G. Magupalli, H. Wu, J. Lieberman, Inflammasome-activated gasdermin D causes pyroptosis by forming membrane pores, Nature 535(7610) (2016) 153-8.
[8] J. Shi, W. Gao, F. Shao, Pyroptosis: Gasdermin-Mediated Programmed Necrotic Cell Death, Trends Biochem Sci 42(4) (2017) 245-254.
[9] M. Kinra, M. Nampoothiri, D. Arora, J. Mudgal, Reviewing the importance of TLR-NLRP3-pyroptosis pathway and mechanism of experimental NLRP3 inflammasome inhibitors, Scand J Immunol 95(2) (2022) e13124.
[10] Y. Huang, W. Xu, R. Zhou, NLRP3 inflammasome activation and cell death, Cell Mol Immunol 18(9) (2021) 2114-2127.
[11] N. Kelley, D. Jeltema, Y. Duan, Y. He, The NLRP3 Inflammasome: An Overview of Mechanisms of Activation and Regulation, Int. J. Mol. Sci 20(13) (2019) 3328.
[12] K.V. Swanson, M. Deng, J.P. Ting, The NLRP3 inflammasome: molecular activation and regulation to therapeutics, Nat. Rev. Immunol 19(8) (2019) 477-489.
[13] S. Paik, J.K. Kim, P. Silwal, C. Sasakawa, E.K. Jo, An update on the regulatory mechanisms of NLRP3 inflammasome activation, Cell Mol Immunol 18(5) (2021) 1141-1160.
[14] R. Munoz-Planillo, P. Kuffa, G. Martinez-Colon, B.L. Smith, T.M. Rajendiran, G. Nunez, K(+) efflux is the common trigger of NLRP3 inflammasome activation by bacterial toxins and particulate matter, Immunity 38(6) (2013) 1142-53.
[15] C.J. Gross, R. Mishra, K.S. Schneider, G. Medard, J. Wettmarshausen, D.C. Dittlein, H. Shi, O. Gorka, P.A. Koenig, S. Fromm, G. Magnani, T. Cikovic, L. Hartjes, J. Smollich, A.A.B. Robertson, M.A. Cooper, M. Schmidt-Supprian, M. Schuster, K. Schroder, P. Broz, C. Traidl-Hoffmann, B. Beutler, B. Kuster, J. Ruland, S. Schneider, F. Perocchi, O. Gross, K(+) Efflux-Independent NLRP3 Inflammasome Activation by Small Molecules Targeting Mitochondria, Immunity 45(4) (2016) 761-773.
[16] Y. Zhang, W. Yang, W. Li, Y. Zhao, NLRP3 Inflammasome: Checkpoint Connecting Innate and Adaptive Immunity in Autoimmune Diseases, Front. Immunol 12 (2021) 732933.
[17] S. Toldo, E. Mezzaroma, L.F. Buckley, N. Potere, M. Di Nisio, G. Biondi-Zoccai, B.W. Van Tassell, A. Abbate, Targeting the NLRP3 inflammasome in cardiovascular diseases, Pharmacol Ther 236 (2022) 108053.
[18] B.R. Sharma, T.D. Kanneganti, NLRP3 inflammasome in cancer and metabolic diseases, Nat Immunol 22(5) (2021) 550-559.

[19] J.A. Holbrook, H.H. Jarosz-Griffiths, E. Caseley, S. Lara-Reyna, J.A. Poulter, C.H. Williams-Gray, D. Peckham, M.F. McDermott, Neurodegenerative Disease and the NLRP3 Inflammasome, Front Pharmacol 12 (2021) 643254.
[20] S.M. Vora, J. Lieberman, H. Wu, Inflammasome activation at the crux of severe COVID-19, Nat. Rev. Immunol 21(11) (2021) 694-703.
[21] C.T. Vong, H.H.L. Tseng, P. Yao, H. Yu, S. Wang, Z. Zhong, Y. Wang, Specific NLRP3 inflammasome inhibitors: promising therapeutic agents for inflammatory diseases, Drug Discov Today 26(6) (2021) 1394-1408.
[22] L. Gonzalez-Cofrade, I. Cuadrado, A. Amesty, A. Estevez-Braun, B. de Las Heras, S. Hortelano, Dehydroisohispanolone as a Promising NLRP3 Inhibitor Agent: Bioevaluation and Molecular Docking, Pharmaceuticals (Basel) 15(7) (2022).
[23] A.G. Atanasov, S.B. Zotchev, V.M. Dirsch, T. International Natural Product Sciences, C.T. Supuran, Natural products in drug discovery: advances and opportunities, Nat Rev Drug Discov 20(3) (2021) 200-216.
[24] M. Huang, J.J. Lu, M.Q. Huang, J.L. Bao, X.P. Chen, Y.T. Wang, Terpenoids: natural products for cancer therapy, Expert Opin Investig Drugs 21(12) (2012) 1801-18.
[25] S.R. Chen, Y. Dai, J. Zhao, L. Lin, Y. Wang, Y. Wang, A Mechanistic Overview of Triptolide and Celastrol, Natural Products from Tripterygium wilfordii Hook F, Front Pharmacol 9 (2018) 104.
[26] J. Xu, E.A. Wold, Y. Ding, Q. Shen, J. Zhou, Therapeutic Potential of Oridonin and Its Analogs: From Anticancer and Antiinflammation to Neuroprotection, Molecules 23(2) (2018).
[27] V. Kishore, N.S. Yarla, A. Bishayee, S. Putta, R. Malla, N.R. Neelapu, S. Challa, S. Das, Y. Shiralgi, G. Hegde, B.L. Dhananjaya, Multi-targeting Andrographolide and its Natural Analogs as Potential Therapeutic Agents, Curr Top Med Chem 17(8) (2017) 845-857.
[28] R.S. Miranda, B. de Jesus, S.R. da Silva Luiz, C.B. Viana, C.R. Adao Malafaia, F.S. Figueiredo, T. Carvalho, M.L. Silva, V.S. Londero, T.A. da Costa-Silva, J.H.G. Lago, R.C.C. Martins, Antiinflammatory activity of natural triterpenes-An overview from 2006 to 2021, Phytother Res 36(4) (2022) 1459-1506.
[29] M.L. Del Prado-Audelo, H. Cortes, I.H. Caballero-Floran, M. Gonzalez-Torres, L. Escutia-Guadarrama, S.A. Bernal-Chavez, D.M. Giraldo-Gomez, J.J. Magana, G. Leyva-Gomez, Therapeutic Applications of Terpenes on Inflammatory Diseases, Front Pharmacol 12 (2021) 704197.
[30] S. Hortelano, L. Gonzalez-Cofrade, I. Cuadrado, B. de Las Heras, Current status of terpenoids as inflammasome inhibitors, Biochem Pharmacol 172 (2020) 113739.
[31] M.T. Islam, S.K. Bardaweel, M.S. Mubarak, W. Koch, K. Gawel-Beben, B. Antosiewicz, J. Sharifi-Rad, Immunomodulatory Effects of Diterpenes and Their Derivatives Through NLRP3 Inflammasome Pathway: A Review, Front Immunol 11 (2020) 572136.

[32] J.A.R. Salvador, A.S. Leal, A.S. Valdeira, B.M.F. Goncalves, D.P.S. Alho, S.A.C. Figueiredo, S.M. Silvestre, V.I.S. Mendes, Oleanane-, ursane-, and quinone methide friedelane-type triterpenoid derivatives: Recent advances in cancer treatment, Eur. J. Med. Chem 142 (2017) 95-130.
[33] J.D. Connolly, R.A. Hill, Triterpenoids, Nat Prod Rep 27(1) (2010) 79-132.
[34] D. Kashyap, A. Sharma, H.S. Tuli, S. Punia, A.K. Sharma, Ursolic Acid and Oleanolic Acid: Pentacyclic Terpenoids with Promising Anti-Inflammatory Activities, Recent Pat Inflamm Allergy Drug Discov 10(1) (2016) 21-33.
[35] A. Villar-Lorenzo, A.E. Ardiles, A.I. Arroba, E. Hernandez-Jimenez, V. Pardo, E. Lopez-Collazo, I.A. Jimenez, I.L. Bazzocchi, A. Gonzalez-Rodriguez, A.M. Valverde, Friedelane-type triterpenoids as selective anti-inflammatory agents by regulation of differential signaling pathways in LPS-stimulated macrophages, Toxicol. Appl. Pharmacol 313 (2016) 57-67.
[36] Z. Li, X. Xiao, M. Yang, Asiatic Acid Inhibits Lipopolysaccharide-Induced Acute Lung Injury in Mice, Inflammation 39(5) (2016) 1642-8.
[37] J. Chen, W. Wu, M. Zhang, C. Chen, Taraxasterol suppresses inflammation in IL-1beta-induced rheumatoid arthritis fibroblast-like synoviocytes and rheumatoid arthritis progression in mice, Int. Immunopharmacol 70 (2019) 274-283.
[38] S.H. Venkatesha, S. Dudics, B. Astry, K.D. Moudgil, Control of autoimmune inflammation by celastrol, a natural triterpenoid, Pathog Dis 74(6) (2016).
[39] W. Xin, Q. Wang, D. Zhang, C. Wang, A new mechanism of inhibition of IL-1beta secretion by celastrol through the NLRP3 inflammasome pathway, Eur J Pharmacol 814 (2017) 240-247.
[40] X. Yu, Q. Zhao, X. Zhang, H. Zhang, Y. Liu, X. Wu, M. Li, X. Li, J. Zhang, X. Ruan, H. Zhang, Celastrol ameliorates inflammation through inhibition of NLRP3 inflammasome activation, Oncotarget 8(40) (2017) 67300-67314.
[41] C. Zhang, M. Zhao, B. Wang, Z. Su, B. Guo, L. Qin, W. Zhang, R. Zheng, The Nrf2-NLRP3-caspase-1 axis mediates the neuroprotective effects of Celastrol in Parkinson's disease, Redox Biol 47 (2021) 102134.
[42] M. Jing, J. Yang, L. Zhang, J. Liu, S. Xu, M. Wang, L. Zhang, Y. Sun, W. Yan, G. Hou, C. Wang, W. Xin, Celastrol inhibits rheumatoid arthritis through the ROS-NF-kappaB-NLRP3 inflammasome axis, Int. Immunopharmacol 98 (2021) 107879.
[43] W. Dai, X. Wang, H. Teng, C. Li, B. Wang, J. Wang, Celastrol inhibits microglial pyroptosis and attenuates inflammatory reaction in acute spinal cord injury rats, Int. Immunopharmacol 66 (2019) 215-223.
[44] C.Y. Yan, S.H. Ouyang, X. Wang, Y.P. Wu, W.Y. Sun, W.J. Duan, L. Liang, X. Luo, H. Kurihara, Y.F. Li, R.R. He, Celastrol ameliorates Propionibacterium acnes/LPS-induced liver damage and MSU-induced gouty arthritis via inhibiting K63 deubiquitination of NLRP3, Phytomedicine 80 (2021) 153398.

[45] Z. Sun, Y. Li, Y. Qian, M. Wu, S. Huang, A. Zhang, Y. Zhang, Z. Jia, Celastrol attenuates ox-LDL-induced mesangial cell proliferation via suppressing NLRP3 inflammasome activation, Cell Death Discov 5 (2019) 114.
[46] S.M. Oramas-Royo, H. Chavez, P. Martin-Rodiguez, L. Fernandez-Perez, A.G. Ravelo, A. Estevez-Braun, Cytotoxic triterpenoids from Maytenus retusa, J. Nat. Prod 73(12) (2010) 2029-34.
[47] N. Giron, E. Perez-Sacau, R. Lopez-Fontal, J.M. Amaro-Luis, S. Hortelano, A. Estevez-Braun, B. de Las Heras, Evaluation of labdane derivatives as potential anti-inflammatory agents, Eur. J. Med. Chem 45(7) (2010) 3155-61.
[48] W. Wang, D. Hu, C. Wu, Y. Feng, A. Li, W. Liu, Y. Wang, K. Chen, M. Tian, F. Xiao, Q. Zhang, M.A. Shereen, W. Chen, P. Pan, P. Wan, K. Wu, J. Wu, STING promotes NLRP3 localization in ER and facilitates NLRP3 deubiquitination to activate the inflammasome upon HSV-1 infection, PLoS Pathog 16(3) (2020) e1008335.
[49] K.V. Swanson, R.D. Junkins, C.J. Kurkjian, E. Holley-Guthrie, A.A. Pendse, R. El Morabiti, A. Petrucelli, G.N. Barber, C.A. Benedict, J.P. Ting, A noncanonical function of cGAMP in inflammasome priming and activation, J Exp Med 214(12) (2017) 3611-3626.
[50] J.P. Green, T. Swanton, L.V. Morris, L.Y. El-Sharkawy, J. Cook, S. Yu, J. Beswick, A.D. Adamson, N.E. Humphreys, R. Bryce, S. Freeman, C. Lawrence, D. Brough, LRRC8A is essential for hypotonicity-, but not for DAMP-induced NLRP3 inflammasome activation, Elife 9 (2020).
[51] R.A. Friesner, R.B. Murphy, M.P. Repasky, L.L. Frye, J.R. Greenwood, T.A. Halgren, P.C. Sanschagrin, D.T. Mainz, Extra precision glide: docking and scoring incorporating a model of hydrophobic enclosure for protein-ligand complexes, J. Med. Chem 49(21) (2006) 6177-96.
[52] R.A. Friesner, J.L. Banks, R.B. Murphy, T.A. Halgren, J.J. Klicic, D.T. Mainz, M.P. Repasky, E.H. Knoll, M. Shelley, J.K. Perry, D.E. Shaw, P. Francis, P.S. Shenkin, Glide: a new approach for rapid, accurate docking and scoring. 1. Method and assessment of docking accuracy, J. Med. Chem 47(7) (2004) 1739-49.
[53] K. Zhu, K.W. Borrelli, J.R. Greenwood, T. Day, R. Abel, R.S. Farid, E. Harder, Docking covalent inhibitors: a parameter free approach to pose prediction and scoring, J Chem Inf Model 54(7) (2014) 1932-40.
[54] S. Mariathasan, D.S. Weiss, K. Newton, J. McBride, K. O'Rourke, M. Roose-Girma, W.P. Lee, Y. Weinrauch, D.M. Monack, V.M. Dixit, Cryopyrin activates the inflammasome in response to toxins and ATP, Nature 440(7081) (2006) 228-32.
[55] Z. Zhaolin, L. Guohua, W. Shiyuan, W. Zuo, Role of pyroptosis in cardiovascular disease, Cell Prolif 52(2) (2019) e12563.
[56] S. Wang, Y.H. Yuan, N.H. Chen, H.B. Wang, The mechanisms of NLRP3 inflammasome/pyroptosis activation and their role in Parkinson's disease, Int. Immunopharmacol 67 (2019) 458-464.

[57] T. Du, J. Gao, P. Li, Y. Wang, Q. Qi, X. Liu, J. Li, C. Wang, L. Du, Pyroptosis, metabolism, and tumor immune microenvironment, Clin Transl Med 11(8) (2021) e492.
[58] A. Di, S. Xiong, Z. Ye, R.K.S. Malireddi, S. Kometani, M. Zhong, M. Mittal, Z. Hong, T.D. Kanneganti, J. Rehman, A.B. Malik, The TWIK2 Potassium Efflux Channel in Macrophages Mediates NLRP3 Inflammasome-Induced Inflammation, Immunity 49(1) (2018) 56-65 e4.
[59] M.S. Dick, L. Sborgi, S. Ruhl, S. Hiller, P. Broz, ASC filament formation serves as a signal amplification mechanism for inflammasomes, Nat Commun 7 (2016) 11929.
[60] N. Kayagaki, I.B. Stowe, B.L. Lee, K. O'Rourke, K. Anderson, S. Warming, T. Cuellar, B. Haley, M. Roose-Girma, Q.T. Phung, P.S. Liu, J.R. Lill, H. Li, J. Wu, S. Kummerfeld, J. Zhang, W.P. Lee, S.J. Snipas, G.S. Salvesen, L.X. Morris, L. Fitzgerald, Y. Zhang, E.M. Bertram, C.C. Goodnow, V.M. Dixit, Caspase-11 cleaves gasdermin D for non-canonical inflammasome signalling, Nature 526(7575) (2015) 666-71.
[61] A.J. Smith, X. Zhang, A.G. Leach, K.N. Houk, Beyond picomolar affinities: quantitative aspects of noncovalent and covalent binding of drugs to proteins, J. Med. Chem 52(2) (2009) 225-33.
[62] J. Singh, R.C. Petter, T.A. Baillie, A. Whitty, The resurgence of covalent drugs, Nat Rev Drug Discov 10(4) (2011) 307-17.
[63] J.G. Robertson, Mechanistic basis of enzyme-targeted drugs, Biochemistry 44(15) (2005) 5561-71.
[64] A. Aljoundi, I. Bjij, A. El Rashedy, M.E.S. Soliman, Covalent Versus Non-covalent Enzyme Inhibition: Which Route Should We Take? A Justification of the Good and Bad from Molecular Modelling Perspective, Protein J 39(2) (2020) 97-105.
[65] A.A. Adeniyi, R. Muthusamy, M.E. Soliman, New drug design with covalent modifiers, Expert Opin Drug Discov 11(1) (2016) 79-90.
[66] G. Glide Software, in: LLC: (Ed.) Schrodinger Suite, LLC, New York, NY, USA, 2021.
[67] T. Rahman, A. Nagar, E.B. Duffy, K. Okuda, N. Silverman, J.A. Harton, NLRP3 Sensing of Diverse Inflammatory Stimuli Requires Distinct Structural Features, Front. Immunol 11 (2020) 1828.
[68] J.A. Duncan, D.T. Bergstralh, Y. Wang, S.B. Willingham, Z. Ye, A.G. Zimmermann, J.P. Ting, Cryopyrin/NALP3 binds ATP/dATP, is an ATPase, and requires ATP binding to mediate inflammatory signaling, Proc. Natl. Acad. Sci. USA 104(19) (2007) 8041-6.
[69] P. Auffinger, F.A. Hays, E. Westhof, P.S. Ho, Halogen bonds in biological molecules, Proc. Natl. Acad. Sci. USA 101(48) (2004) 16789-94.